


Weak, homogeneous turbulence with rotation and stratification: a numerical study of the non-propagating component

Julian F. Scott¹  and Claude Cambon¹

¹Laboratoire de Mécanique des Fluides et d'Acoustique, Université de Lyon, Ecole Centrale de Lyon, 36 avenue Guy de Collongue, Ecully CEDEX 69134, France

Corresponding author: Julian F. Scott, julian.scott@ec-lyon.fr

(Received 8 February 2025; revised 26 June 2025; accepted 28 June 2025)

Following Scott & Cambon (2024 *J. Fluid Mech.* vol. 979, A17), henceforth referred to as [I], a spectral approach is used and the flow is expressed as a sum of normal modes, which are of two types: inertial/gravity waves and non-propagating (NP) modes. It was shown in [I] that, for weak (small Rossby or Froude number) turbulence, the NP component of the flow decouples from the waves at leading order and here we focus on the NP part alone. It is demonstrated that the evolution equations of the NP component are equivalent to the three-dimensional, quasi-geostrophic (QG) approximation of geophysical fluid dynamics. For QG turbulence, the seminal paper of Charney (1971 *J. Atmos. Sci.* vol. 28, pp. 1087–1095), referred to as [II], concluded that, as for two-dimensional turbulence, the energy cascade for QG turbulence should go from smaller to larger scales and that the inertial-range spectrum at wavenumber k should behave as k^{-3} . He also proposed that the energy distribution in spectral space is isotropic if the vertical wavenumber is appropriately scaled and deduced a principle of equipartition in which the average kinetic energy is twice the potential one. We use Charney's transformation of spectral coordinates to effectively eliminate the parameter $\beta = 2\Omega/N$, where Ω is the rotation rate and N the Brunt–Vaisala frequency, and give results of numerical calculations concerning the energy distribution. The results mostly agree with [II] at large enough times, although they do not support Charney isotropy. They further suggest self-similarity of the time evolution of the three-dimensional energy distribution in spectral space away from the vertical axis.

Key words: homogeneous turbulence, rotating turbulence, stratified turbulence

1. Introduction

This paper concerns weak, freely decaying, homogeneous turbulence subject to rotation, represented by Ω , and stable stratification, expressed by a constant Brunt–Vaisala frequency, N . The approach used is a spectral one, i.e. based on Fourier transforms, and a general overview of homogeneous turbulence with this viewpoint in mind can be found in the book by Sagaut & Cambon (2018). By weak turbulence, we mean that either the Rossby number, $u'/\Omega L$, or Froude number, u'/NL , is small, where u' and L are measures of the turbulent velocity and the size of its large scales.

This article uses the formulation of Scott & Cambon (2024) (henceforth referred to as [I]) as a basis. We should note that the restriction to a small wave/non-propagating (NP) amplitude ratio of [I] was lifted in Scott (2025). As in [I], the flow is expressed as a linear combination of modes, each a solution of the governing equations without nonlinearity or visco-diffusion, which form a complete set capable of representing general solenoidal velocity fields. The modes are of two types: oscillatory ones which represent inertial/gravity waves and time-independent ones, referred to as NP because they have zero frequency, hence zero group velocity. It was shown in [I] that, for weak turbulence, the NP component of the flow decouples from the wave one at leading order and can thus be studied on its own, which is what we do here.

As was noted in [I] and demonstrated in this article, the governing equations of the NP component of weak turbulence are equivalent to the three-dimensional, quasi-geostrophic (QG) approximation, which is widely used in geophysical applications and has a long history. Thus, the present work applies directly to QG turbulence. The QG approximation was first proposed by Charney (1948), whose later publication, Charney (1971) (henceforth referred to as [II]), is perhaps the most influential article in the area of QG turbulence and will be referred to on multiple occasions in what follows. Although now rather dated, the review by Rhines (1979) provides an overview of QG turbulence. Since the parameter $\beta = 2\Omega/N$ is usually small for atmospheric and oceanic flows, such smallness is sometimes implicit in geophysical studies, whereas small β is not supposed here. Note that the notation $\beta = 2\Omega/N$, used in the present article, has no connection with the geophysical β -plane, used to approximate a spherical Earth. There is no β -plane effect here.

The work in [II] drew a formal analogy between QG turbulence and the physically different problem of two-dimensional turbulence (without rotation or stratification). Two-dimensional turbulence has been the subject of much work (see the review by Boffetta & Ecke (2012)). Perhaps the most important conclusion is that there are two cascades. Energy goes from small to large scales, while enstrophy (one half the mean squared vorticity) is transferred in the opposite direction. In the isotropic case, each cascade is associated with a power law for the energy spectrum: $k^{-5/3}$ for the energy cascade and k^{-3} for enstrophy, where k is the wavenumber. Thus, if external forcing is applied at a particular wavenumber and the Reynolds number is large, one expects $k^{-5/3}$ below that wavenumber and k^{-3} above it. Transfer of enstrophy towards smaller scales eventually encounters viscosity, producing a range of k above the k^{-3} one in which the enstrophy flux is dissipated and the spectrum falls off rapidly. For freely decaying turbulence, the enstrophy cascade leads to a k^{-3} inertial range, while the energy cascade produces growth in the size of the large scales. Given that the energy transfer is towards the larger scales, one expects that energy dissipation is small at large Reynolds number, in principle going to zero at infinite Reynolds number, hence energy conservation in the inviscid case.

For QG turbulence, which is three-dimensional, [II] suggested that a quantity known as potential enstrophy plays much the same role in the QG problem as enstrophy does in the two-dimensional one. As a result, he proposed two cascades, with energy going towards larger scales and potential enstrophy towards smaller ones. The work in [II] concluded that

energy should be nearly conserved and that the energy spectrum should have an inertial range in which it behaves as k^{-3} . He also proposed that the energy distribution in spectral space is isotropic when expressed using coordinates in which the vertical wavenumber is multiplied by β . Note that such ‘Charney isotropy’ does not imply isotropy in the usual sense unless $\beta = 1$. Thus, when $\beta < 1$, Charney isotropy leads to a vertically elongated energy distribution, while, for $\beta > 1$, the predicted distribution extends further in the horizontal than in the vertical direction. Charney isotropy makes the energy distribution axisymmetric and implies the result that the average kinetic energy should be twice the potential one, a condition sometimes known as Charney equipartition.

Charney’s suggestion of isotropy was supported by the numerical simulations of QG turbulence by Hua & Haidvogel (1986) and McWilliams (1989), of whom the latter also demonstrated the similarities of QG and two-dimensional turbulence regarding cascades and their directions. More recent simulations by Vallgren & Lindborg (2010) also support the predictions of [II]. As we shall see, our results agree with most of the proposals of [II], but not isotropy. This is one of the notable conclusions of this article. Another being self-similarity of the time evolution of the distribution of energy in spectral space at large enough times and away from the vertical axis.

The article by Smith & Waleffe (2002) is representative of studies of rotating/stratified turbulence using full direct numerical simulation. It is based on the Boussinesq equations, rather than the QG ones used here and considers forced turbulence, rather the freely decaying case which is the subject of this article. Only limited comparisons with [II] are made.

Although we focus on energy, we should observe that QG flows are rich in structures such as vortices, and the statistics of these have been explored by, for instance, McWilliams (1990), McWilliams, Weiss & Yavneh (1999), Dritschel, de la Torre Juarez & Ambaum (1999), von Hardenberg *et al.* (2000) and Reinaud, Dritschel & Koudella (2003). However, in this article we concentrate on the energy and its distribution in spectral space.

This paper is organised as follows. Section 2 describes the theoretical basis, the weak-turbulence limit and its relationship with the QG approximation and a transformation of variables which essentially removes the parameter β from consideration. Finally, § 3 gives numerical results.

2. Formulation

Consider freely decaying homogeneous turbulence in an unbounded, incompressible, rotating, stably stratified fluid having constant density, constant Brunt–Vaisala frequency, N , and constant rotation vector, $\boldsymbol{\Omega}$, which is supposed parallel to gravity and has unit vector $\mathbf{e} = \boldsymbol{\Omega}/\Omega$, where $\Omega = |\boldsymbol{\Omega}|$. Henceforth, spatial coordinates, time and velocity are non-dimensionalised using L , $(N^2 + 4\Omega^2)^{-1/2}$ and $L(N^2 + 4\Omega^2)^{1/2}$, where L is a length scale characterising the large scales of the initial turbulence.

2.1. Analytical background

Using a rotating frame of reference and Cartesian coordinates, as well as the summation convention, the non-dimensional Boussinesq equations of motion are

$$\frac{\partial u_i}{\partial t} + \widehat{\Omega} \varepsilon_{ijk} e_j u_k + \widehat{N} \eta e_i + \frac{\partial p}{\partial x_i} = - \frac{\partial}{\partial x_j} (u_i u_j) + D_u \frac{\partial^2 u_i}{\partial x_j \partial x_j}, \quad (2.1)$$

$$\frac{\partial u_i}{\partial x_i} = 0, \quad (2.2)$$

$$\frac{\partial \eta}{\partial t} - \widehat{N} e_i u_i = - \frac{\partial}{\partial x_j} (\eta u_j) + D_\eta \frac{\partial^2 \eta}{\partial x_j \partial x_j}, \quad (2.3)$$

where ε_{ijk} is the alternating tensor, $\widehat{\Omega} = 2\Omega(N^2 + 4\Omega^2)^{-1/2}$ and $\widehat{N} = N(N^2 + 4\Omega^2)^{-1/2}$. Furthermore, $D_u = \nu(N^2 + 4\Omega^2)^{-1/2}L^{-2}$ and $D_\eta = \kappa(N^2 + 4\Omega^2)^{-1/2}L^{-2}$, where ν is the kinematic viscosity and κ the diffusivity associated with the buoyancy variable η . Note that $\widehat{N} = (\beta^2 + 1)^{-1/2}$ and $\widehat{\Omega} = \beta(\beta^2 + 1)^{-1/2}$, where $\beta = \widehat{\Omega}/\widehat{N} = 2\Omega/N$. Thus, the non-dimensional governing equations, (2.1)–(2.3), only depend on the parameters β , D_u and D_η . For simplicity's sake, $\widehat{\Omega}$, \widehat{N} are denoted Ω , N in what follows. Because we will only be working with non-dimensional quantities, this should not lead to confusion. Note that the right-hand sides of (2.1) and (2.3) express nonlinearity, viscosity and diffusion. The visco-diffusive terms dissipate energy.

As described in [I], in the absence of nonlinearity and visco-diffusion, (2.1)–(2.3) have particular solutions, referred to as modes, which are indexed by an integer $s = 0, \pm 1$ and a wave vector \mathbf{k} . Modes have the velocity and buoyancy variable

$$u_i = v_i^{(s)}(\mathbf{k}) \exp(i(\mathbf{k} \cdot \mathbf{x} - s\omega(\mathbf{k})t)), \quad (2.4)$$

$$\eta = \eta^{(s)}(\mathbf{k}) \exp(i(\mathbf{k} \cdot \mathbf{x} - s\omega(\mathbf{k})t)), \quad (2.5)$$

where the notation \cdot represents a scalar product,

$$\omega(\mathbf{k}) = (N^2 \sin^2 \theta + \Omega^2 \cos^2 \theta)^{1/2}, \quad (2.6)$$

where θ is the angle between \mathbf{k} and the rotation vector and $v_i^{(s)}$, $\eta^{(s)}$ are given by (1.2.12)–(1.2.15) (where, here and henceforth, (I.x.y) refers to equation (x.y) of [I]).

Although modes do not allow for nonlinearity or visco-diffusion, they form a complete set for $u_i(\mathbf{x})$, $\eta(\mathbf{x})$ satisfying (2.2). Thus, the flow can be expressed at any given time as

$$u_i = \sum_{s=0,\pm 1} u_{i,s}, \quad \eta = \sum_{s=0,\pm 1} \eta_s, \quad (2.7)$$

where

$$u_{i,s} = \int a_s(\mathbf{k}, t) v_i^{(s)}(\mathbf{k}) \exp(i(\mathbf{k} \cdot \mathbf{x} - s\omega(\mathbf{k})t)) d^3 \mathbf{k}, \quad (2.8)$$

$$\eta_s = \int a_s(\mathbf{k}, t) \eta^{(s)}(\mathbf{k}) \exp(i(\mathbf{k} \cdot \mathbf{x} - s\omega(\mathbf{k})t)) d^3 \mathbf{k}, \quad (2.9)$$

and a_s are the mode amplitudes at time t . The a_s evolve in time due to nonlinearity and visco-diffusion.

Equations (2.7)–(2.9) express the flow as a linear combination of modes indexed by $s = 0, \pm 1$ and the wave vector \mathbf{k} , each mode being a solution of the governing equations without visco-diffusion and nonlinearity of the form $\exp(i(\mathbf{k} \cdot \mathbf{x} - s\omega(\mathbf{k})t))$. The modes with $s = \pm 1$ are inertial-gravity waves, whose dispersion relation is (2.6). The non-dimensionalisation of time makes the period of oscillation of such waves of order 1. The mode $s = 0$ has zero frequency, hence zero group velocity. Thus, the corresponding component of the flow is indeed non-propagating, hence its designation by NP. As in [I], since u_i and η are real, $a_s(-\mathbf{k}) = a_{-s}^*(\mathbf{k})$, where $*$ denotes complex conjugation. Using the identities $v_i^{(s)}(-\mathbf{k}) = v_i^{(-s)*}(\mathbf{k})$, $\eta^{(s)}(-\mathbf{k}) = \eta^{(-s)*}(\mathbf{k})$ and $\omega(-\mathbf{k}) = \omega(\mathbf{k})$, (2.8) and (2.9) imply $u_{i,s} = u_{i,-s}^*$, $\eta_s = \eta_{-s}^*$. Thus, the NP component, defined by $u_i^{NP} = u_{i,0}$ and $\eta^{NP} = \eta_0$, is real, whereas $s = +1$ and $s = -1$ provide conjugate contributions to (2.7), whose sum is the wave component and is also real.

According to (I.2.26), the evolution of the modal amplitudes is described by

$$\frac{\partial a_s}{\partial t} = -ik_j(v_i^{(s)*} \widetilde{u_i u_j} + \eta^{(s)*} \widetilde{\eta u_j}) \exp(is\omega t) - \sum_{\hat{s}=0, \pm 1} D_{s\hat{s}} \exp(i(s - \hat{s})\omega t) a_{\hat{s}}, \quad (2.10)$$

where $s = 0, \pm 1$,

$$\tilde{f}(\mathbf{k}) = \frac{1}{8\pi^3} \int f(\mathbf{x}) \exp(-i\mathbf{k} \cdot \mathbf{x}) d^3\mathbf{x} \quad (2.11)$$

defines spatial Fourier transformation and $D_{s\hat{s}}$ is the Hermitian, positive definite matrix given by (I.2.20) and which represents visco-diffusion.

Since we want to study turbulent flow, a statistical ensemble of flow realisations is introduced, as well as ensemble averaging. The flow is assumed to have initial statistics which are homogeneous with respect to spatial translation, a property which is preserved by time evolution according to the governing equations, (2.1)–(2.3). The flow is also assumed to be initially of zero mean, i.e. $\overline{u_i} = 0$ and $\overline{\eta} = 0$, where the overbars denote ensemble averaging. Given homogeneity, this property is also preserved by (2.1)–(2.3). Here, $\overline{u_i} = 0$, $\overline{\eta} = 0$ can be shown to imply $\overline{a_s} = 0$ and $\overline{u_{i,s}} = \overline{\eta_s} = 0$. Thus, a_s and both the wave and NP components of the flow have zero mean.

Given the statistical homogeneity of the flow, the second-order moments of the modal amplitudes have the form

$$\overline{a_s^*(\mathbf{k}) a_{s'}(\mathbf{k}')} = A_{ss'}(\mathbf{k}) \delta(\mathbf{k} - \mathbf{k}'), \quad (2.12)$$

where $A_{ss'}$ is a Hermitian, positive semidefinite matrix, referred to as the spectral matrix. Since $a_s(-\mathbf{k}) = a_{-s}^*(\mathbf{k})$, $A_{ss'}(-\mathbf{k}) = A_{-s', -s}(\mathbf{k})$. The average non-dimensional energy per unit volume in physical space is

$$\underbrace{\frac{1}{2} \overline{u_i u_i}}_{\text{Kinetic}} + \underbrace{\frac{1}{2} \overline{\eta^2}}_{\text{Potential}} = \int e(\mathbf{k}) d^3\mathbf{k}, \quad (2.13)$$

where

$$e(\mathbf{k}) = \frac{1}{2} \sum_{s=0, \pm 1} A_{ss}(\mathbf{k}) \quad (2.14)$$

is the energy density in spectral space. Equation (2.14) indicates that the diagonal elements of $A_{ss'}$ yield the contribution, $A_{ss}/2$, of mode \mathbf{k} , s to the energy density. Given that $A_{ss'}$ is Hermitian and positive semidefinite, the modal energy contribution is real and non-negative. The off-diagonal elements of $A_{ss'}$ can be complex and represent correlations between modes of different s . The spectral energy density can be split into wave and NP contributions as $e = e_W + e_{NP}$, where

$$e_W = \frac{1}{2} \sum_{s=\pm 1} A_{ss}, \quad e_{NP} = \frac{1}{2} A_{00}. \quad (2.15)$$

Since $A_{ss'}(-\mathbf{k}) = A_{-s', -s}(\mathbf{k})$, $e_W(-\mathbf{k}) = e_W(\mathbf{k})$ and $e_{NP}(-\mathbf{k}) = e_{NP}(\mathbf{k})$. The NP contribution to the average energy per unit volume is

$$E_{NP} = \underbrace{\frac{1}{2} \overline{u_i^{NP} u_i^{NP}}}_{\text{Kinetic}} + \underbrace{\frac{1}{2} \overline{\eta^{NP2}}}_{\text{Potential}} = \int e_{NP}(\mathbf{k}) d^3\mathbf{k}. \quad (2.16)$$

The subject of this article being the NP component of the flow, we note that

$$v_1^{(0)} = \frac{ik_2}{(k_1^2 + k_2^2 + \beta^2 k_3^2)^{1/2}}, \quad v_2^{(0)} = -\frac{ik_1}{(k_1^2 + k_2^2 + \beta^2 k_3^2)^{1/2}}, \quad v_3^{(0)} = 0, \quad (2.17)$$

$$\eta^{(0)} = \frac{i\beta k_3}{(k_1^2 + k_2^2 + \beta^2 k_3^2)^{1/2}} \quad (2.18)$$

follow from (I.2.12), (I.2.13), (I.2.15) and $\beta = \Omega/N$, where, here and henceforth, x_1 and x_2 are horizontal coordinates, while x_3 is vertical (so $\mathbf{e} = (0, 0, 1)$). We also note that the NP mode damping coefficient is

$$D_{00} = k^2 \frac{D_u(k_1^2 + k_2^2) + D_\eta \beta^2 k_3^2}{k_1^2 + k_2^2 + \beta^2 k_3^2}, \quad (2.19)$$

according to (I.2.15) and (I.2.20), where $k = |\mathbf{k}|$. Observe that (2.8) and (2.17) imply that the NP velocity, $u_i^{NP} = u_{i,0}$, is horizontal and divergence free.

2.2. Weak turbulence and the QG approximation

From here on, we suppose that the turbulence is weak (small Rossby or Froude number). Given the temporal oscillations of the wave modes, it is shown in [I] (§ 3.1) that (2.10) with $s = 0$ has the leading-order approximation

$$\frac{\partial a_0}{\partial t} + D_{00}a_0 = -ik_j \left(v_i^{(0)*} \widetilde{u_i^{NP} u_j^{NP}} + \eta^{(0)*} \widetilde{\eta^{NP} u_j^{NP}} \right), \quad (2.20)$$

where, from (2.8) and (2.9),

$$u_i^{NP}(\mathbf{x}) = \int a_0(\mathbf{k}) v_i^{(0)}(\mathbf{k}) \exp(i\mathbf{k} \cdot \mathbf{x}) d^3 \mathbf{k}, \quad (2.21)$$

$$\eta^{NP}(\mathbf{x}) = \int a_0(\mathbf{k}) \eta^{(0)}(\mathbf{k}) \exp(i\mathbf{k} \cdot \mathbf{x}) d^3 \mathbf{k}, \quad (2.22)$$

are the NP velocity and scalar fields in physical space ($u_i^{NP} = u_{i,0}$ and $\eta^{NP} = \eta_0$). Equations (2.20)–(2.22) govern the time evolution of $a_0(\mathbf{k})$ and indicate that the NP component is decoupled from the wave component in the weak-turbulence limit. As discussed in [I] following equation (I.3.6), this arises due to temporal oscillations of the integrand in that equation apart from near the surface $\omega(\mathbf{p}) = \omega(-\mathbf{k} - \mathbf{p})$ when $s_p = -s_q$ and the vanishing of $M_{0,s,-s}(\mathbf{k}, \mathbf{p})$ on that surface. Thus, for weak turbulence, the effect of the wave component on evolution of the NP one is negligible. We only consider the NP component from here onwards. Observe that (2.20)–(2.22) depend on the parameter β via (2.17)–(2.19). Leaving aside the visco-diffusive term, $D_{00}a_0$, in (2.20), β is the only parameter of the problem.

It was noted in [I] that (2.20)–(2.22) are equivalent to the three-dimensional QG equations used in geophysical applications. This is demonstrated in Appendix A, where it is shown that (2.20) can be re-expressed as

$$\frac{\partial a_0}{\partial t} + D_{00}a_0 = -i(k_1^2 + k_2^2 + \beta^2 k_3^2)^{-1/2} k_j \widetilde{u_j^{NP} q}, \quad (2.23)$$

where

$$q(\mathbf{x}) = \int (k_1^2 + k_2^2 + \beta^2 k_3^2)^{1/2} a_0(\mathbf{k}) \exp(i\mathbf{k} \cdot \mathbf{x}) d^3 \mathbf{k}, \quad (2.24)$$

is the potential vorticity. Equations (2.21), (2.23) and (2.24) are equivalent to (2.20)–(2.22) and provide a somewhat simpler expression of the evolution equations of $a_0(\mathbf{k})$. In particular, using (2.23), rather than (2.20), the numerical calculation of the nonlinear term is considerably less time consuming. Note that $\overline{q^2}/2$ is the potential enstrophy, which was referred to in the introduction.

Let ε_{NP} be a small, positive parameter characterising the weakness of turbulence, hence u_i^{NP} , η^{NP} and q are $O(\varepsilon_{NP})$. Introducing the $O(1)$ scaled variables $\hat{u}_i = \varepsilon_{NP}^{-1} u_i^{NP}$, $\hat{\eta} = \varepsilon_{NP}^{-1} \eta^{NP}$ and $\hat{q} = \varepsilon_{NP}^{-1} q$, (2.21)–(2.24) give

$$\frac{\partial \hat{a}}{\partial \hat{t}} + \hat{D} \hat{a} = -i(k_1^2 + k_2^2 + \beta^2 k_3^2)^{-1/2} k_j \widetilde{\hat{u}_j \hat{q}}, \quad (2.25)$$

$$\hat{u}_i(\mathbf{x}) = \int \hat{a}(\mathbf{k}) v_i^{(0)}(\mathbf{k}) \exp(i\mathbf{k} \cdot \mathbf{x}) d^3 \mathbf{k}, \quad (2.26)$$

$$\hat{q}(\mathbf{x}) = \int (k_1^2 + k_2^2 + \beta^2 k_3^2)^{1/2} \hat{a}(\mathbf{k}) \exp(i\mathbf{k} \cdot \mathbf{x}) d^3 \mathbf{k}, \quad (2.27)$$

$$\hat{\eta}(\mathbf{x}) = \int \hat{a}(\mathbf{k}) \eta^{(0)}(\mathbf{k}) \exp(i\mathbf{k} \cdot \mathbf{x}) d^3 \mathbf{k}, \quad (2.28)$$

where $\hat{a} = \varepsilon_{NP}^{-1} a_0$ and $\hat{D} = \varepsilon_{NP}^{-1} D_{00}$, while $\hat{t} = \varepsilon_{NP} t$ is the appropriate time variable for evolution of the NP component. Equations (2.25)–(2.27) are the evolution equations for $\hat{a}(\mathbf{k})$ which form the basis of the present work. The second term on the left-hand side of (2.25) represents visco-diffusion, whereas the right-hand side expresses nonlinearity. The scaled version of e_{NP} is $\hat{e} = \varepsilon_{NP}^{-2} e_{NP}$ and yields the scaled energy per unit volume via

$$\hat{E}_{NP} = \underbrace{\frac{1}{2} \overline{\hat{u}_i \hat{u}_i}}_{\text{Kinetic}} + \underbrace{\frac{1}{2} \overline{\hat{\eta}^2}}_{\text{Potential}} = \int \hat{e}(\mathbf{k}) d^3 \mathbf{k}. \quad (2.29)$$

The quantity ε_{NP} is chosen such that the initial scaled energy per unit volume is 1. Thus,

$$\varepsilon_{NP}^2 = \int e_{NP}(\mathbf{k}, \hat{t} = 0) d^3 \mathbf{k}, \quad (2.30)$$

provides a precise definition of ε_{NP} .

There is a particular case for which (2.25) takes a very simple form. This is when the vector \mathbf{k} is parallel to the vertical axis, i.e. $k_1 = k_2 = 0$. As noted above, \mathbf{u}^{NP} is horizontal so $\hat{u}_3 = 0$, hence $k_j \widetilde{\hat{u}_j \hat{q}} = 0$ when $k_1 = k_2 = 0$. Thus, the nonlinear term in (2.25) is zero and linear theory holds. It follows that $\hat{e}(\mathbf{k}, \hat{t}) = \hat{e}(\mathbf{k}, 0) \exp(-2\hat{D}(\mathbf{k})\hat{t})$ for vertical \mathbf{k} .

2.3. The partial elimination of β

The evolution equations (2.25)–(2.27) depend on the parameter β , both directly and via (2.17) and (2.19). This dependency can be almost entirely removed by a change of the variables \mathbf{k} and \hat{a} , as follows.

Adopting the change of variables

$$\hat{k}_1 = k_1, \quad \hat{k}_2 = k_2, \quad \hat{k}_3 = \beta k_3, \quad (2.31)$$

equations (2.17) and (2.18) imply

$$v_1^{(0)} = i \frac{\hat{k}_2}{\hat{k}}, \quad v_2^{(0)} = -i \frac{\hat{k}_1}{\hat{k}}, \quad v_3^{(0)} = 0, \quad \eta^{(0)} = \frac{i \hat{k}_3}{\hat{k}}, \quad (2.32)$$

where $\widehat{k} = |\widehat{\mathbf{k}}|$. This shows that $v_i^{(0)}(\widehat{\mathbf{k}})$ and $\eta^{(0)}(\widehat{\mathbf{k}})$ are independent of β . Introducing

$$\widehat{x}_1 = x_1, \quad \widehat{x}_2 = x_2, \quad \widehat{x}_3 = \beta^{-1} x_3, \quad (2.33)$$

then (2.11) gives $\tilde{f}(\mathbf{k}) = \beta \tilde{f}(\widehat{\mathbf{k}})$, where

$$\tilde{f}(\widehat{\mathbf{k}}) = \frac{1}{8\pi^3} \int f(\widehat{\mathbf{x}}) \exp(-i\widehat{\mathbf{k}} \cdot \widehat{\mathbf{x}}) d^3\widehat{\mathbf{x}}, \quad (2.34)$$

and we have used $\mathbf{k} \cdot \mathbf{x} = \widehat{\mathbf{k}} \cdot \widehat{\mathbf{x}}$ and $d^3\mathbf{x} = \beta d^3\widehat{\mathbf{x}}$. Since $\hat{u}_3 = 0$, $k_j \widetilde{\hat{u}}_j \hat{q} = \widehat{k}_j \widetilde{\hat{u}}_j \hat{q} = \beta \widehat{k}_j \widetilde{\hat{u}}_j \hat{q}$, hence (2.25) gives

$$\frac{\partial \widehat{a}}{\partial \hat{t}} + \widehat{D}\widehat{a} = -i\widehat{k}^{-1} \widehat{k}_j \widetilde{\hat{u}}_j \hat{q}, \quad (2.35)$$

where $\widehat{a}(\widehat{\mathbf{k}}) = \beta^{-1} \hat{a}(\mathbf{k})$. Using $\mathbf{k} \cdot \mathbf{x} = \widehat{\mathbf{k}} \cdot \widehat{\mathbf{x}}$ and $d^3\mathbf{k} = \beta^{-1} d^3\widehat{\mathbf{k}}$, (2.26)–(2.28) imply

$$\hat{u}_i(\widehat{\mathbf{x}}) = \int \widehat{a}(\widehat{\mathbf{k}}) v_i^{(0)}(\widehat{\mathbf{k}}) \exp(i\widehat{\mathbf{k}} \cdot \widehat{\mathbf{x}}) d^3\widehat{\mathbf{k}}, \quad (2.36)$$

$$\hat{q}(\widehat{\mathbf{x}}) = \int \widehat{k} \widehat{a}(\widehat{\mathbf{k}}) \exp(i\widehat{\mathbf{k}} \cdot \widehat{\mathbf{x}}) d^3\widehat{\mathbf{k}}, \quad (2.37)$$

$$\hat{\eta}(\widehat{\mathbf{x}}) = \int \widehat{a}(\widehat{\mathbf{k}}) \eta^{(0)}(\widehat{\mathbf{k}}) \exp(i\widehat{\mathbf{k}} \cdot \widehat{\mathbf{x}}) d^3\widehat{\mathbf{k}}, \quad (2.38)$$

and, according to (2.19),

$$\widehat{D}(\widehat{\mathbf{k}}) = (\widehat{k}_1^2 + \widehat{k}_2^2 + \beta^{-2} \widehat{k}_3^2) \frac{\widehat{D}_u(\widehat{k}_1^2 + \widehat{k}_2^2) + \widehat{D}_\eta \widehat{k}_3^2}{\widehat{k}^2}, \quad (2.39)$$

where $\widehat{D}_u = \varepsilon_{NP}^{-1} D_u$ and $\widehat{D}_\eta = \varepsilon_{NP}^{-1} D_\eta$. Note that the time variable, \hat{t} , is not modified by the above changes of variables: only $\widehat{k}_3 = \beta k_3$ and $\widehat{a}(\widehat{\mathbf{k}}) = \beta^{-1} \hat{a}(\mathbf{k})$ need to be borne in mind.

Equations (2.34)–(2.37) and (2.39) describe the time evolution of $\widehat{a}(\widehat{\mathbf{k}})$. The parameter β only appears via (2.39), which gives the visco-diffusive damping coefficient of NP modes. Thus, in the absence of visco-diffusive dissipation, β has been eliminated from the NP evolution problem. As usual in studies of turbulence, dissipation is supposed negligible for the large scales, becoming important only for very small ones (the dissipative scales). Thus, we expect the β -dependency of (2.39) to affect sufficiently small scales, but not the large- or inertial-range ones which are the focus of this work. In fact, the only reason for including dissipation is to avoid numerical instabilities which tend to arise otherwise.

Equation (2.29) and $d^3\mathbf{k} = \beta^{-1} d^3\widehat{\mathbf{k}}$ yield

$$\widehat{E}_{NP} = \underbrace{\frac{1}{2} \widetilde{\hat{u}}_i \hat{u}_i}_{\text{Kinetic}} + \underbrace{\frac{1}{2} \widetilde{\hat{\eta}}^2}_{\text{Potential}} = \int \widehat{e}(\widehat{\mathbf{k}}) d^3\widehat{\mathbf{k}}, \quad (2.40)$$

where $\widehat{e}(\widehat{\mathbf{k}}) = \beta^{-1} \hat{e}(\mathbf{k})$ is the energy density in $\widehat{\mathbf{k}}$ -space. Since $e_{NP}(-\mathbf{k}) = e_{NP}(\mathbf{k})$, $\widehat{e}(-\widehat{\mathbf{k}}) = \widehat{e}(\widehat{\mathbf{k}})$. Also, $\widehat{E}_{NP}(\hat{t} = 0) = 1$ implies that the initial energy density should satisfy

$$\int \widehat{e}(\widehat{\mathbf{k}}, \hat{t} = 0) d^3\widehat{\mathbf{k}} = 1. \quad (2.41)$$

The energy density can be written as the sum, $\widehat{e} = \widehat{e}_K + \widehat{e}_P$, of kinetic and potential contributions, which are given by

$$\widehat{e}_K(\widehat{\mathbf{k}}) = \frac{\widehat{k}_1^2 + \widehat{k}_2^2}{\widehat{k}^2} \widehat{e}(\widehat{\mathbf{k}}), \quad \widehat{e}_P(\widehat{\mathbf{k}}) = \frac{\widehat{k}_3^2}{\widehat{k}^2} \widehat{e}(\widehat{\mathbf{k}}), \quad (2.42)$$

and determine the scaled kinetic and potential energies per unit volume via

$$\widehat{E}_K = \frac{1}{2} \overline{\widehat{u}_i \widehat{u}_i} = \int \widehat{e}_K(\widehat{\mathbf{k}}) d^3 \widehat{\mathbf{k}}, \quad \widehat{E}_P = \frac{1}{2} \overline{\widehat{\eta}^2} = \int \widehat{e}_P(\widehat{\mathbf{k}}) d^3 \widehat{\mathbf{k}}. \quad (2.43)$$

Note that [II] proposed isotropy of $\widehat{e}(\widehat{\mathbf{k}})$ in $\widehat{\mathbf{k}}$ -space, giving the equipartition relation $\widehat{E}_K = 2\widehat{E}_P$ according to (2.42) and (2.43).

3. Numerical method and results

The method used to solve (2.34)–(2.37) is described in Appendix B and is similar to that of classical direct numerical simulation (DNS) of homogeneous turbulence. Thus, given \widehat{a} at some time \widehat{t} , numerical approximation of the Fourier transforms in (2.36) and (2.37) is used to determine \widehat{u}_j and \widehat{q} in physical space. The product $\widehat{u}_j \widehat{q}$ is then taken and a numerical Fourier transform used to approximate the right-hand side of (2.35).

As noted above, as usual in studies of turbulence, dissipation is supposed small for the large scales, while increasing in significance for smaller ones and becoming important in a dissipative range of large \widehat{k} . We suppose that the precise form, (2.39), of the dissipative damping factor, $\widehat{D}(\widehat{\mathbf{k}})$, is unimportant as regards the large- and inertial-range scales studied here. In the hope of extending the inertial range to higher \widehat{k} than would be the case using (2.39), a hyperviscous damping factor, $\widehat{D}(\widehat{\mathbf{k}}) = d\widehat{k}^6$, is used in the numerical calculations (see e.g. Haugen & Brandenburg (2004) for a discussion of hyperviscous methods). The use of a hyperviscosity completely removes the β -dependence. The hyperviscosity, d , is a numerical parameter and a small value is required for small dissipation of the large scales. The value of d and of all other numerical parameters are given at the end of Appendix B.

Although the present approach is applicable in the general case, we henceforth specialise to turbulence which is statistically axisymmetric, i.e. the flow statistics are unchanged by rotation about the vertical axis. Like statistical homogeneity, this symmetry is preserved by the governing equations. Thus, if the statistics are initially axisymmetric, as is the case for the results reported below, they remain so. Statistical axisymmetry implies $\widehat{e}(\widehat{\mathbf{k}}) = \widehat{e}(\widehat{k}_\perp, \widehat{k}_3)$, where $\widehat{k}_\perp = (\widehat{k}_1^2 + \widehat{k}_2^2)^{1/2}$ is the transverse wavenumber, hence $\widehat{e}(\widehat{k}_\perp, -\widehat{k}_3) = \widehat{e}(\widehat{k}_\perp, \widehat{k}_3)$ follows from $\widehat{e}(-\widehat{\mathbf{k}}) = \widehat{e}(\widehat{\mathbf{k}})$. For this reason, only results for $\widehat{k}_3 \geq 0$ are given in what follows.

Various measures of the NP energy and its spectral distribution are used to present the results, including $\widehat{e}(\widehat{\mathbf{k}})$, the total energy, \widehat{E}_{NP} , and its kinetic and potential components, \widehat{E}_K and \widehat{E}_P . The energy distributions with respect to \widehat{k} , \widehat{k}_\perp and \widehat{k}_3 are expressed by the $\widehat{\mathbf{k}}$ -space surface integrals

$$\Phi(\widehat{k}) = \int_{|\widehat{\mathbf{k}}|=\widehat{k}} \widehat{e}(\widehat{\mathbf{k}}) d^2 \widehat{\mathbf{k}}, \quad (3.1)$$

$$\Phi_\perp(\widehat{k}_\perp) = \int_{(\widehat{k}_1^2 + \widehat{k}_2^2)^{1/2} = \widehat{k}_\perp} \widehat{e}(\widehat{\mathbf{k}}) d^2 \widehat{\mathbf{k}}, \quad (3.2)$$

$$\Phi_\parallel(\widehat{k}_3) = \int_{\widehat{\mathbf{k}} \cdot \mathbf{e} = \widehat{k}_3} \widehat{e}(\widehat{\mathbf{k}}) d^2 \widehat{\mathbf{k}}, \quad (3.3)$$

each of which gives the total energy via

$$\hat{E}_{NP} = \int_0^\infty \Phi(\hat{k}) d\hat{k} = \int_0^\infty \Phi_\perp(\hat{k}_\perp) d\hat{k}_\perp = \int_{-\infty}^\infty \Phi_\parallel(\hat{k}_3) d\hat{k}_3. \quad (3.4)$$

The quantities ℓ , ℓ_\perp and ℓ_\parallel , defined by

$$\begin{pmatrix} \ell^{-1} \\ \ell_\perp^{-1} \\ \ell_\parallel^{-1} \end{pmatrix} = \hat{E}_{NP}^{-1} \int \begin{pmatrix} \hat{k} \\ \hat{k}_\perp \\ |\hat{k}_3| \end{pmatrix} \hat{e}(\hat{\mathbf{k}}) d^3\hat{\mathbf{k}}, \quad (3.5)$$

express different measures of the size of the large scales. The numerical approximation of \hat{e} , \hat{E}_{NP} , \hat{E}_K , \hat{E}_P and the quantities defined by (3.1)–(3.3) and (3.5) is described in Appendix B.

The numerical procedure requires the initial energy density, $\hat{e}(\hat{\mathbf{k}}, \hat{t} = 0)$, which should satisfy (2.41). We begin using

$$\hat{e}(\hat{\mathbf{k}}, \hat{t} = 0) = \frac{2}{3\pi^{3/2}} \hat{k}^2 e^{-\hat{k}^2}, \quad (3.6)$$

the aim being to place the dominant initial energy in the large scales. We expect an initial phase in which energy is transferred towards small scales and inertial and dissipative ranges are formed. We study this phase, as well as the subsequent development. As noted in the introduction, we expect energy transfer towards large scales at later times. Equation (3.6) makes the initial energy distribution isotropic in $\hat{\mathbf{k}}$ -space (although not in \mathbf{k} -space unless $\beta = 1$). This type of isotropy is the one envisaged in [II] and earlier referred to as Charney isotropy. We will later consider two other initial energy density distributions. Note that (3.6) is consistent with the assumption of statistical axisymmetry made earlier.

Before giving results, we note some limitations of the numerical method used. Firstly, the quantities of interest, for instance the spectral energy density, are ensemble averages, whose accurate calculation using DNS would require very many realisations of the flow with different, randomly chosen, initial conditions. However, this would entail an impracticably large computational cost. Thus, as is usual in DNS, we consider the results of single realisations, in the hope that they represent the average. For this reason, random fluctuations are to be expected in the results. A second limitation of DNS is the discretisation in spectral space.

Figure 1 shows the evolution of $\Phi(\hat{k})$ during the initial stages. As expected, nonlinear transfer from large to small scales leads to a power-law inertial range and the formation of a dissipative one. At lower values of \hat{k} , the random fluctuations due to using a single realisation are apparent, as is discretisation. These artefacts of the numerics are also present in subsequent results, although we will only mention them when they have significant implications. At the end of the given time range, $\hat{t} = 5$, having established the dissipative range and brought the inertial range to near equilibrium, one might be tempted to stop the calculation, but, in fact, this is far from the end of the story. A clue that this might be the case is the power law, \hat{k}^{-4} , rather than the expected \hat{k}^{-3} .

Figure 2 shows the evolution of Φ at longer times. The spectral peak moves towards smaller \hat{k} , corresponding to increasing size of the large scales due to transfer of energy from smaller to larger ones, a process often referred to as an inverse energy cascade. The power law in the inertial range starts off as \hat{k}^{-4} , but later approaches the expected \hat{k}^{-3} . The decrease of the total energy, \hat{E}_{NP} , is only approximately 3% between the initial instant and $\hat{t} = 50$, which is much later than the time of formation of the dissipative range

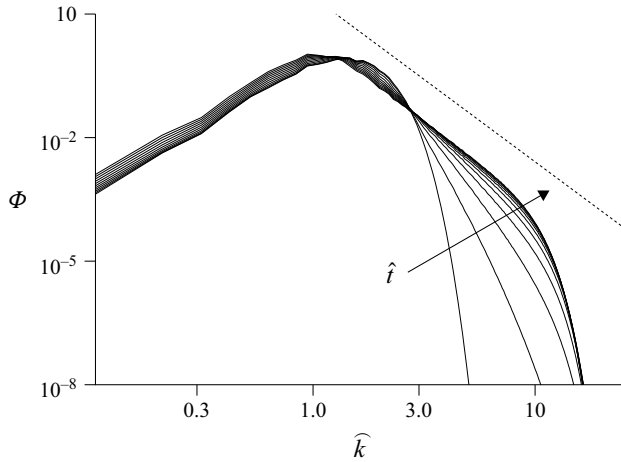


Figure 1. Log-log plots of $\Phi(\hat{k})$ for eleven values of \hat{t} , equally spaced from $\hat{t} = 0$ to $\hat{t} = 5$. The dashed line represents the power law \hat{k}^{-4} .

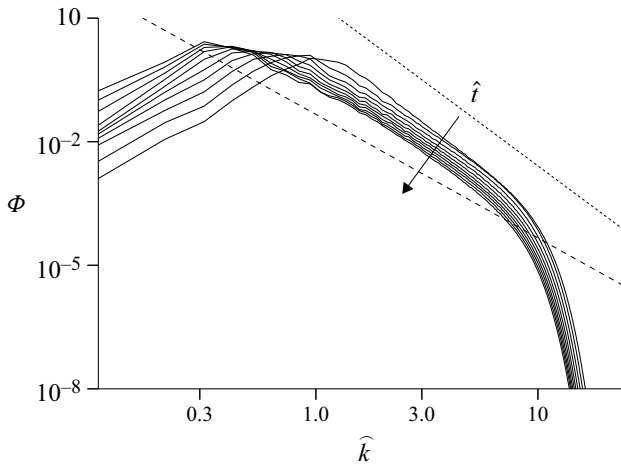


Figure 2. Log-log plots of $\Phi(\hat{k})$ for ten values of \hat{t} , equally spaced from $\hat{t} = 5$ to $\hat{t} = 50$. The finely dashed line represents the power law \hat{k}^{-4} , whereas the more coarsely dashed one represents \hat{k}^{-3} .

(see figure 1). As discussed in [I], this suggests that there is no energy cascade towards smaller scales, hence energy conservation in the limit in which the visco-diffusion tends to zero. The growth in size of the large scales, the lack of a forward energy cascade and the \hat{k}^{-3} power law are each consistent with [II].

The numerical determination of the kinetic and potential components, \hat{E}_K and \hat{E}_P , of the energy is described in Appendix B. Given (3.6), their initial values are $\hat{E}_K = 2/3$ and $\hat{E}_P = 1/3$, hence initial Charney equipartition, $\hat{E}_K = 2\hat{E}_P$. To our surprise, \hat{E}_K and \hat{E}_P showed little time dependence, \hat{E}_K increasing slightly to $\hat{E}_K = 0.693$ and \hat{E}_P decreasing a little to $\hat{E}_P = 0.276$ at $\hat{t} = 50$. Thus, Charney equipartition persists approximately to later times.

Figure 3 shows the evolution of Φ at still longer times. By $\hat{t} = 100$, the spectral peak has moved to such low \hat{k} that the spectral discretisation of DNS is important. This places

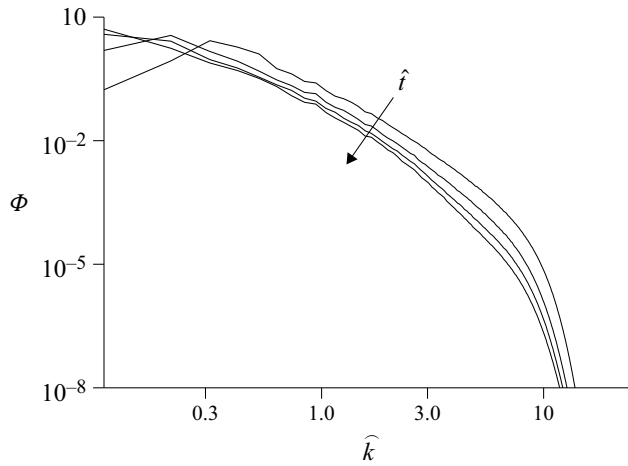


Figure 3. Log-log plots of $\Phi(\hat{k})$ for four values of \hat{t} , equally spaced from $\hat{t} = 50$ to $\hat{t} = 200$.

a limit on how large \hat{t} can be before the numerical calculation loses credibility. For this reason, we mostly restrict our attention to $\hat{t} \leq 50$ in what follows.

Returning to the time range of figure 2, we consider the regime in which \hat{k}^{-3} applies in the inertial range. This requires sufficiently large \hat{t} , say $\hat{t} > 20$. Figure 4(a) shows $\ell^{-1}\Phi$ as a function of $\hat{k}\ell$ for different times, where $\ell(\hat{t})$ is given by (3.5). The motivation for using $\hat{k}\ell$ is to compensate for the growth in the size of the large scales, a size represented by ℓ , while the introduction of $\ell^{-1}\Phi$ is based on the first equation of (3.4) and the observed near constancy of \hat{E}_{NP} . Comparing figure 4(a) with figure 2, and leaving aside the dissipative range, use of the scaled variables $\ell^{-1}\Phi$ and $\hat{k}\ell$ considerably reduces the differences between the three times $\hat{t} = 25$, $\hat{t} = 37.5$ and $\hat{t} = 50$, while the results differ significantly in the dissipative range. These results suggest that $\Phi(\hat{k})$ is self-similar for large- and inertial-range wavenumbers, but not for the dissipative range. The case $\hat{t} = 5$, indicated by the dashed curve in figure 4(a), is included to show that self-similarity requires sufficiently large \hat{t} . Figures 4(b) and 4(c) show similar results for Φ_{\perp} and Φ_{\parallel} , which also appear to be self-similar for large enough \hat{t} . Note that the same length scale, $\ell(\hat{t})$, is used for all three spectra, Φ , Φ_{\perp} and Φ_{\parallel} . Similar conclusions are reached if ℓ_{\perp} or ℓ_{\parallel} is used instead of ℓ .

Self-similarity of Φ , Φ_{\perp} and Φ_{\parallel} suggests that the three-dimensional energy distribution, $\hat{e}(\hat{\mathbf{k}})$, is itself self-similar, i.e.

$$\hat{e} = \ell^3 F(\hat{k}_{\perp}\ell, \hat{k}_3\ell), \quad (3.7)$$

where the factor ℓ^3 arises from (2.40) and energy conservation. As noted above, we only expect self-similarity for large- and inertial-range scales at sufficiently large \hat{t} . Figure 5 shows contour plots of $\ell^{-3}\hat{e}$ in the $\hat{k}_{\perp}\ell$ – $\hat{k}_3\ell$ plane for $\hat{t} = 25$ and $\hat{t} = 50$. The wiggles in the curves are due to the use of a single realisation. The results for the two times are quite close, apart from near the vertical axis, $\hat{k}_{\perp}\ell = 0$, which suggests that $\hat{e}(\hat{\mathbf{k}})$ is indeed self-similar away from that axis. Note, however, that it does not appear to be isotropic. In particular, the inertial-range energy distribution clearly extends further in the vertical direction than in the horizontal one. This is the point on which our results disagree with [II].

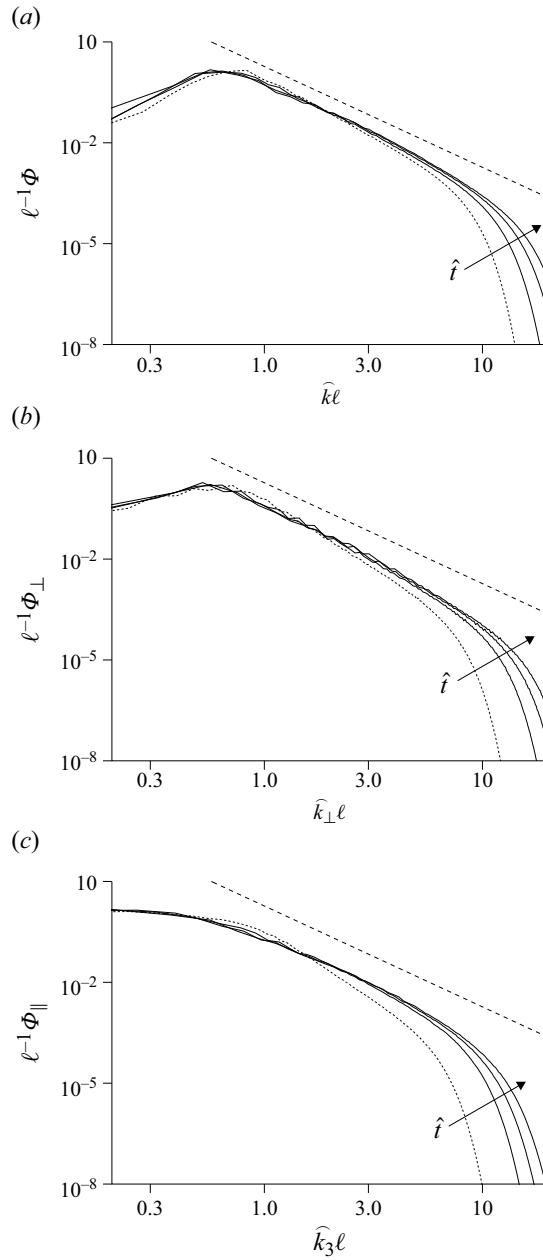


Figure 4. Log-log plots of (a) $\ell^{-1}\Phi$ as a function of $\hat{k}\ell$, (b) $\ell^{-1}\Phi_{\perp}$ as a function of $\hat{k}_{\perp}\ell$ and (c) $\ell^{-1}\Phi_{\parallel}$ as a function of $\hat{k}_3\ell$ for four values of \hat{t} . The dashed curves are for $\hat{t}=5$, while the continuous curves are for $\hat{t}=25$, $\hat{t}=37.5$ and $\hat{t}=50$. The dashed straight lines represent power laws with exponent -3 . The arrows indicate the direction of increasing \hat{t} for the dissipative range.

Several reasons may explain the near-axis differences between $\hat{t}=25$ and $\hat{t}=50$ apparent in figure 5. Firstly, the numerical determination of $\hat{e}(\hat{\mathbf{k}})$, described in Appendix B, involves arithmetic averaging over small annular regions and the number of terms in the average decreases as the axis is approached, leading to increased random fluctuations,

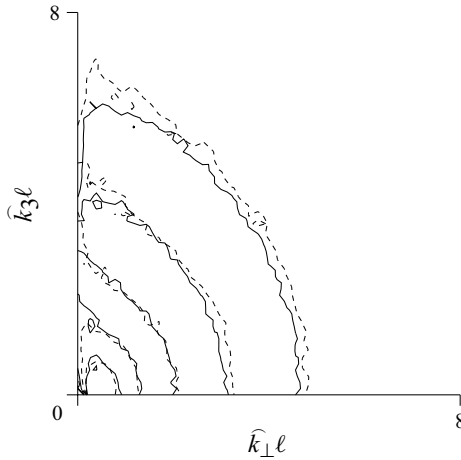


Figure 5. Contours of constant $\ell^{-3}\hat{e}$. There are five contours representing the values $\ell^{-3}\hat{e} = 10^{-5}$, $\ell^{-3}\hat{e} = 10^{-4}$, $\ell^{-3}\hat{e} = 10^{-3}$, $\ell^{-3}\hat{e} = 10^{-2}$ and $\ell^{-3}\hat{e} = 10^{-1}$. The continuous curves are for the time $\hat{t} = 25$, while the dashed ones correspond to $\hat{t} = 50$.

as observed. Secondly, as discussed at the end of § 2.2, for $\hat{\mathbf{k}}$ on the axis, $\hat{e}(\hat{\mathbf{k}})$ takes the value given by linear theory, a value which is close to (3.6) because large-scale dissipation is very small. Thus, the axial value cannot participate in the self-similar evolution which appears to apply away from the axis. This suggests that there is a near-axial region, perhaps decreasing in extent as \hat{t} increases, in which self-similarity of $\hat{e}(\hat{\mathbf{k}})$ does not apply.

The results given up to now are for the initial conditions (3.6) and we now consider the more general ones

$$\hat{e}(\hat{\mathbf{k}}, \hat{t} = 0) = \frac{2}{3\pi^{3/2}} \alpha^{1/2} X e^{-X}, \quad (3.8)$$

where $X = \alpha \hat{k}_\perp^2 + \alpha^{-1} \hat{k}_3^2$ and $\alpha > 0$ is a parameter that controls the ratio of the vertical and horizontal spectral extents of the initial energy density. The value $\alpha = 1$ leads to (3.6), the isotropic initial energy distribution considered previously, whereas the initial conditions are anisotropic for other values of α . The multiplicative factor $\alpha^{1/2}$ in (3.8) ensures that the condition (2.41) is satisfied. Like (3.6), (3.8) is consistent with statistical axisymmetry.

Calculations were performed for the two values $\alpha = 1/2$ and $\alpha = 2$ and results similar to figures 1–4 obtained. Here, \hat{E}_{NP} was again found to be nearly constant. As noted earlier, when $\alpha = 1$, the initial Charney equipartition of kinetic and potential energies is nearly preserved following time evolution. Figure 6 shows \hat{E}_K and \hat{E}_P as functions of time for $\alpha = 1/2$ and $\alpha = 2$. Although starting well away from it, they evolve towards approximate equipartition. Thus, when it is not initially present, equipartition is approached, but, like the k^{-3} power law and self-similarity, takes some time to develop. Furthermore, the end results only approximate exact Charney equipartition.

Figure 7 compares $\hat{t} = 50$ contours of $\ell^{-3}\hat{e}$ for $\alpha = 1/2$ and $\alpha = 2$ with those for $\alpha = 1$. There is quite close agreement of $\alpha = 1/2$ with $\alpha = 1$ away from the vertical axis. The disagreement appears to extend further from the axis for $\alpha = 2$, but, away from the axis, there does not appear to be a strong dependency on the initial conditions.

Figure 8 shows $\ell(\hat{t})$, $\ell_\perp(\hat{t})$ and $\ell_\parallel(\hat{t})$ for $\alpha = 1/2$, $\alpha = 1$ and $\alpha = 2$. Although the results for the different values of α are significantly different in the initial stages, the differences

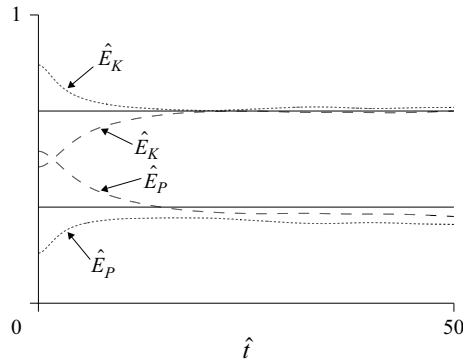


Figure 6. Plots of \hat{E}_K and \hat{E}_P as functions of time for $\alpha = 1/2$ (finely dashed curves) and $\alpha = 2$ (coarsely dashed curves). The two continuous horizontal lines represent the equipartition values, $1/3$ and $2/3$.

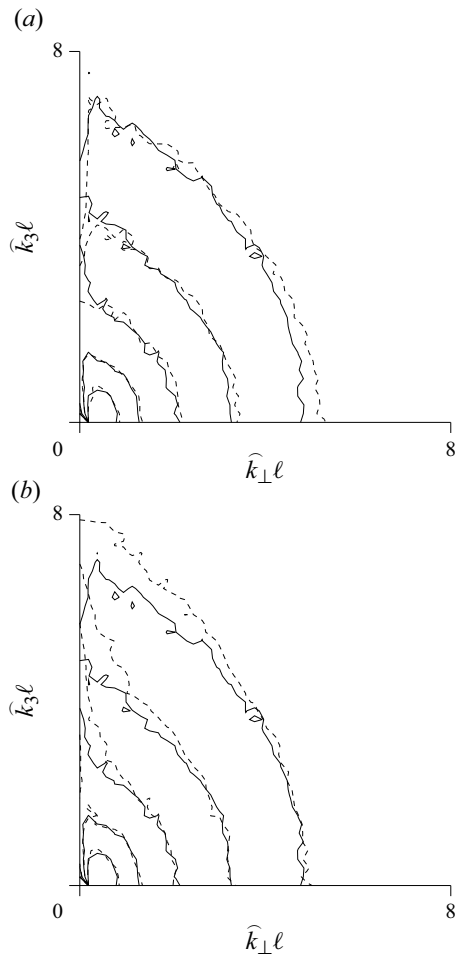


Figure 7. Contours of constant $\ell^{-3}\hat{e}$ for $\hat{t} = 50$ and (a) $\alpha = 1$ and $\alpha = 1/2$, (b) $\alpha = 1$ and $\alpha = 2$. The continuous curves are for $\alpha = 1$, while the dashed ones are for $\alpha = 1/2$ and $\alpha = 2$. There are five contours representing the values $\ell^{-3}\hat{e} = 10^{-5}$, $\ell^{-3}\hat{e} = 10^{-4}$, $\ell^{-3}\hat{e} = 10^{-3}$, $\ell^{-3}\hat{e} = 10^{-2}$ and $\ell^{-3}\hat{e} = 10^{-1}$.

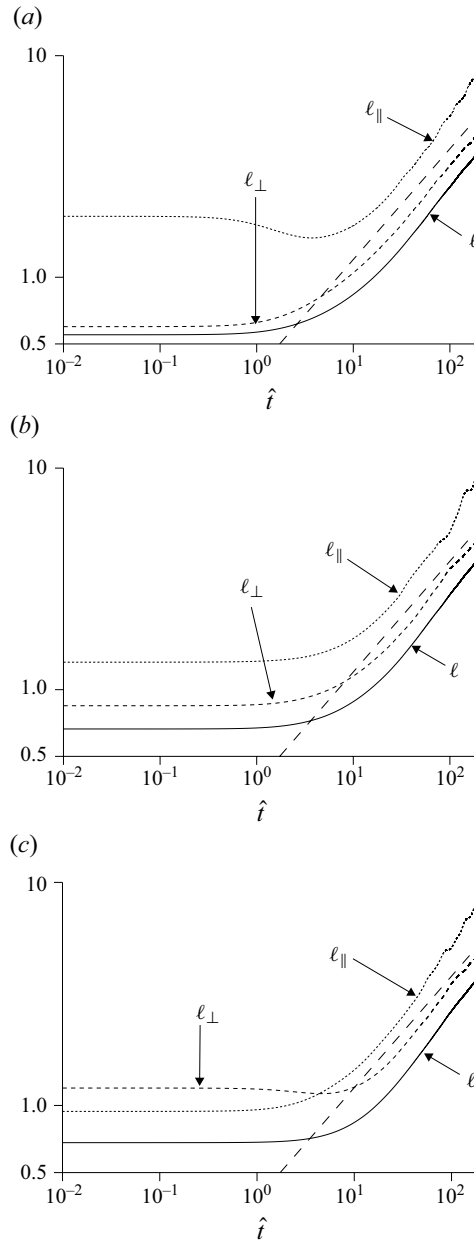


Figure 8. Log-log plots of ℓ , ℓ_{\perp} and ℓ_{\parallel} as functions of \hat{t} up to $\hat{t} = 200$ for (a) $\alpha = 1/2$, (b) $\alpha = 1$ and (c) $\alpha = 2$. The dashed straight lines represent the power law $\hat{t}^{1/2}$.

are rather minor for large enough \hat{t} . It should, however, be borne in mind that, as noted earlier, the numerical results lose credibility due to discretisation when \hat{t} is too large. This is no doubt the case towards the right-hand end of figure 8 and may explain the oscillations of $\ell_{\parallel}(\hat{t})$ apparent there. For the larger values of \hat{t} , $\ell(\hat{t})$, $\ell_{\perp}(\hat{t})$ and $\ell_{\parallel}(\hat{t})$ are all increasing, corresponding to the increasing size of the large scales. An approximate power law of $\hat{t}^{1/2}$ is apparent. We note that such a square-root time dependence has been reported for

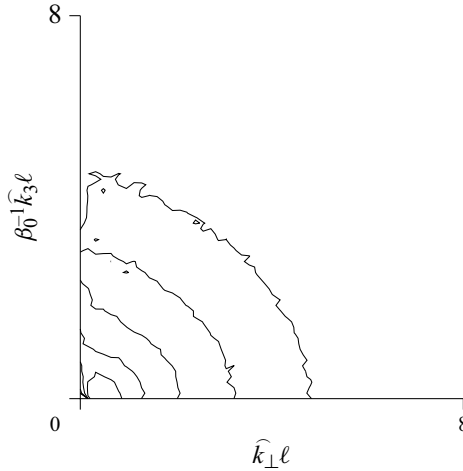


Figure 9. Contours of constant $\ell^{-3}\hat{e}$ in the $\hat{k}_\perp\ell - \beta_0^{-1}\hat{k}_3\ell$ plane for $\alpha = 1$, $\hat{t} = 37.5$ and $\beta_0 = 1.4$. There are five contours representing the values $\ell^{-3}\hat{e} = 10^{-5}$, $\ell^{-3}\hat{e} = 10^{-4}$, $\ell^{-3}\hat{e} = 10^{-3}$, $\ell^{-3}\hat{e} = 10^{-2}$ and $\ell^{-3}\hat{e} = 10^{-1}$.

two-dimensional turbulence, see Lowe & Davidson (2005), but, to our knowledge, has not yet been explained theoretically.

Given the results described thus far, it is plausible that, at sufficiently large \hat{t} and in the absence of numerical approximations, the energy density in $\hat{\mathbf{k}}$ -space has the self-similar form (3.7) for large- and inertial-range scales away from the vertical axis. Equation (3.7) implies

$$\hat{e} = \beta \ell^3 F(k_\perp \ell, \beta k_3 \ell), \quad (3.9)$$

for the energy density in \mathbf{k} -space, where $k_\perp = (k_1^2 + k_2^2)^{1/2}$. Given that, with the exception of the dissipative range, the parameter β was eliminated by the transformations of § 2.3, the functions F and $\ell(\hat{t})$ are independent of β . Further assuming, as suggested by our results, that these functions are independent of the initial conditions, they are universal. Equation (3.9) indicates that changing β does not essentially modify the energy distribution. The spectral extent with respect to k_3 varies proportional to β^{-1} , while the multiplicative factor, $\beta \ell^3$, maintains the value $\hat{E}_{NP} = 1$. As $\beta \rightarrow 0$, the purely stratified case is approached and the spectral extent with respect to k_3 is large, corresponding to near horizontal stratification. Likewise, as $\beta \rightarrow \infty$, the purely rotating case is approached and the energy density is concentrated near $k_3 = 0$, hence vertically orientated structures dominate. Increasing \hat{t} causes $\ell(\hat{t})$ to increase, corresponding to growth in size of the large scales. Each of these results might be expected on physical grounds, but (3.9) makes more precise, quantitative predictions, expressing self-similarity, universality and energy conservation.

Turning attention to the inertial range, as noted earlier, the self-similar energy density appears to be anisotropic in $\hat{\mathbf{k}}$ -space, extending further in \hat{k}_3 than in \hat{k}_\perp . This suggests that it could be brought closer to isotropy by a multiplicative rescaling of \hat{k}_3 . Figure 9 shows contours of $\ell^{-3}\hat{e}$ in the $\hat{k}_\perp\ell - \beta_0^{-1}\hat{k}_3\ell$ plane for $\alpha = 1$, $\hat{t} = 37.5$ and $\beta_0 = 1.4$. The result is approximately isotropic away from the vertical axis and we henceforth consider the consequences of supposing isotropy of \hat{e} following such rescaling of \hat{k}_3 . Given such isotropy, (3.7) implies

$$F(\hat{k}_\perp\ell, \hat{k}_3\ell) = f((\hat{k}_\perp^2 + \beta_0^{-2}\hat{k}_3^2)^{1/2}\ell). \quad (3.10)$$

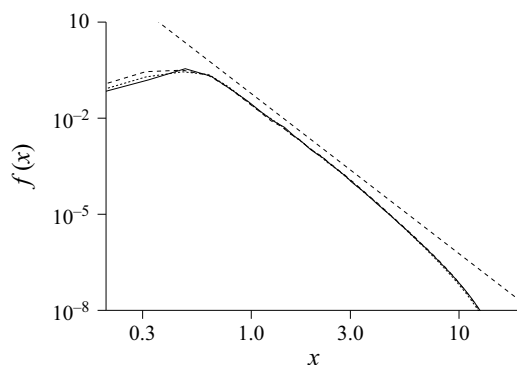


Figure 10. Log-log plot of $f(x)$ obtained using results for $\hat{t} = 37.5$. The continuous curve is for $\alpha = 1$, the finely dashed one for $\alpha = 1/2$ and the more coarsely dashed one for $\alpha = 2$. The dashed straight line represents the power law x^{-5} .

The numerical determination of the function $f(x)$ is described in [Appendix B](#) and results are given in [figure 10](#). The near coincidence of the results for the different values of α supports the suggestion that the self-similar energy density does not depend on the initial conditions. An x^{-5} power law is apparent, hence $f(x) \sim Cx^{-5}$, which implies

$$\hat{e} = C\ell^{-2}(\hat{k}_{\perp}^2 + \beta_0^{-2}\hat{k}_3^2)^{-5/2}, \quad (3.11)$$

for the inertial range, away from the vertical axis, where the constant C has the approximate value $C = 0.03$. Equation (3.11) leads to power laws of exponent -3 for Φ , Φ_{\perp} and Φ_{\parallel} , agreeing with results given earlier. It also implies

$$\hat{e} = C\beta\ell^{-2} \left(k_{\perp}^2 + \left(\frac{\beta}{\beta_0} \right)^2 k_3^2 \right)^{-5/2}, \quad (3.12)$$

hence inertial-range isotropy in \mathbf{k} -space when $\beta = \beta_0$. Such isotropy is in agreement with the results of [I] for $\beta = 1.4$ (see figure 1e of that article). Indeed, this was the reason for the choice, $\beta_0 = 1.4$, in [figure 9](#). Anisotropy for other values of β is apparent from (3.12) and figure 1 of [I]. Note that we have no theoretical explanation of the value $\beta_0 = 1.4$.

4. Conclusions

4.1. Discussion

This article has been devoted to weak, freely decaying, homogeneous turbulence subject to rotation and stratification. The flow is expressed as a linear combination of wave and NP modes and the weak-turbulence result of [I], that the NP component decouples from the wave one at leading order, used to restrict attention to the NP component. The NP modal amplitude, $a_0(\mathbf{k})$, where \mathbf{k} is the wave vector in spectral space, evolves according to (2.20)–(2.22). It was shown that these equations are equivalent to (2.21), (2.23) and (2.24), which are those of three-dimensional, QG turbulence. Thus, our results apply directly to QG turbulence.

The turbulent energy, which has kinetic and potential components, can be written as the sum of wave and NP contributions. Given statistical homogeneity, the second-order

moments of the NP modal amplitudes have the form

$$\overline{a_0^*(\mathbf{k})a_0(\mathbf{k}')} = A_{00}(\mathbf{k})\delta(\mathbf{k} - \mathbf{k}'), \quad (4.1)$$

where A_{00} is real, non-negative and such that $A_{00}(-\mathbf{k}) = A_{00}(\mathbf{k})$. The NP part of the energy density in spectral space is $e_{NP}(\mathbf{k}) = A_{00}(\mathbf{k})/2$ and gives the total, average NP energy per unit volume in physical space, E_{NP} , via (2.16).

Since the turbulence is weak, a_0 is small. A parameter ε_{NP} , given by (2.30), was introduced as a measure of weakness and used to scale the modal amplitude as $\hat{a} = \varepsilon_{NP}^{-1}a_0$ and time as $\hat{t} = \varepsilon_{NP}t$. Corresponding scalings of e_{NP} and E_{NP} are $\hat{e} = \varepsilon_{NP}^{-2}e_{NP}$ and $\hat{E}_{NP} = \varepsilon_{NP}^{-2}E_{NP}$, which are related by (2.29). Equation (2.30) means that the scalings are such that $\hat{E}_{NP} = 1$ at the initial instant, $\hat{t} = 0$.

Following scaling, the evolution equations are (2.25)–(2.27). These equations depend on the parameter β , a dependency which is almost entirely removed by a change of the variables \mathbf{k} and \hat{a} . Choosing coordinates such that x_1 and x_2 are horizontal, while x_3 is vertical, the new wave vector $\hat{\mathbf{k}}$, where $\hat{k}_1 = k_1$, $\hat{k}_2 = k_2$ and $\hat{k}_3 = \beta k_3$, is used to describe position in spectral space, whereas the NP modal amplitude is described by $\hat{a}(\hat{\mathbf{k}}) = \beta^{-1}\hat{a}(\mathbf{k})$. These variable transformations lead to the evolution equations (2.34)–(2.37), equations which only depend on β via the visco-diffusive (dissipative) coefficient, \hat{D} , of (2.35). This remaining dependency is apparent from (2.39). The energy density in $\hat{\mathbf{k}}$ -space is $\hat{e}(\hat{\mathbf{k}}) = \beta^{-1}\hat{e}(\mathbf{k})$ and gives \hat{E}_{NP} via (2.40). The kinetic and potential contributions to \hat{e} are given by (2.42). Note that [III] postulated isotropy of $\hat{e}(\hat{\mathbf{k}})$. If such isotropy is supposed, the equipartition relation that the average kinetic energy be twice the potential one follows from (2.42) and (2.43).

The energy density $\hat{e}(\hat{\mathbf{k}})$ and a number of other measures of the energy distribution in $\hat{\mathbf{k}}$ -space were used to present the results. The spectra $\Phi(\hat{k})$, $\Phi_{\perp}(\hat{k}_{\perp})$ and $\Phi_{\parallel}(\hat{k}_3)$, where $\hat{k} = |\hat{\mathbf{k}}|$ and $\hat{k}_{\perp} = (\hat{k}_1^2 + \hat{k}_2^2)^{1/2}$, are given by (3.1)–(3.3) and represent the distributions of energy over \hat{k} , \hat{k}_{\perp} and \hat{k}_3 , as indicated by (3.4). The quantities $\ell(\hat{t})$, $\ell_{\perp}(\hat{t})$ and $\ell_{\parallel}(\hat{t})$ are defined by (3.5) and are measures of the size of the large scales.

As noted above, (2.34)–(2.37) depend on β via the visco-diffusive term of (2.35). However, as usual in studies of turbulence, visco-diffusive dissipation is supposed negligible for the large scales, becoming important only for very small ones (the dissipative scales). Thus, we expect the β -dependency of (2.39) to affect sufficiently small scales, but not the large- or inertial-range ones, which are the focus of this work. In fact, the only reason for including dissipation is to avoid numerical instabilities which tend to arise otherwise. We suppose that the precise form, (2.39), of the dissipative damping factor, $\hat{D}(\hat{\mathbf{k}})$, is unimportant as regards the large- and inertial-range scales studied here. In the hope of extending the inertial range to higher \hat{k} than would be the case using (2.39), a hyperviscous damping factor, $\hat{D}(\hat{\mathbf{k}}) = d\hat{k}^6$, is used in the numerical calculations. The use of a hyperviscosity completely removes the β -dependence. The hyperviscosity, d , is a numerical parameter and a small value is required for small dissipation of the large scales. We used $d = 10^{-6}$.

Having replaced the visco-diffusive term by a hyperviscous one, (2.34)–(2.37) are solved numerically as described in Appendix B. The method is similar to that of classical DNS of homogeneous turbulence. Thus, given \hat{a} at some time \hat{t} , numerical approximation of the Fourier transforms in (2.36) and (2.37) is used to determine \hat{u}_j and \hat{q} in physical space. The product $\hat{u}_j\hat{q}$ is then taken and a numerical Fourier transform used to approximate the right-hand side of (2.35).

When considering results, two limitations of the numerical method should be borne in mind. Firstly, the quantities of interest are ensemble averages, whose accurate calculation using DNS would require very many realisations of the flow with different, randomly chosen, initial conditions. However, this would entail an impracticably large computational cost. Thus, as is usual in DNS, we consider the results of single realisations, in the hope that they represent the average. For this reason, random fluctuations are to be expected in the results. A second limitation of DNS is the discretisation in spectral space.

4.2. Results

Turning attention to the results, we first undertook a calculation with the initial energy density (3.6). Figures 1–3 show the resulting $\Phi(\hat{k})$ at different times. In the early stages (figure 1), energy transfer from large to small scales leads to an inertial, then a dissipative range. At the end of this stage, there is a \hat{k}^{-4} power law in the inertial range. In figure 2, the spectral peak moves towards lower \hat{k} , indicating a growth in size of the large scales, while the inertial-range power law changes gradually from \hat{k}^{-4} to \hat{k}^{-3} . There is only a slight decrease, 3 %, of \hat{E}_{NP} between the initial instant, $\hat{t} = 0$, and $\hat{t} = 50$, which is much later than that ($\hat{t} \sim 5$) required for formation of the dissipative range. Such near energy conservation suggests that there is no forward energy cascade. The growth in size of the large scales, the lack of a forward energy cascade and the \hat{k}^{-3} power law are each consistent with [II]. However, as the transition from \hat{k}^{-4} to \hat{k}^{-3} shows, attaining the regime in which the results of [II] hold requires sufficiently long times (say $\hat{t} > 20$), considerably longer than those for formation of the inertial and dissipative ranges.

Figure 3 shows the evolution of Φ at later times and indicates that the spectral discretisation of DNS becomes important due to the growth in size of the large scales. This places a limit on how large \hat{t} can be before the numerical calculation loses credibility. For this reason, we mostly restrict our attention to $\hat{t} \leq 50$.

Figure 4(a) shows $\ell^{-1}(\hat{t})\Phi$ as a function of $\hat{k}\ell(\hat{t})$ for times $\hat{t} = 5$, $\hat{t} = 25$, $\hat{t} = 37.5$ and $\hat{t} = 50$. Here, $\hat{k}\ell$ is used to suppress the growth of the large scales noted above, while $\ell^{-1}\Phi$ is suggested by energy conservation. For $\hat{t} = 25$, $\hat{t} = 37.5$ and $\hat{t} = 50$, the use of these variables considerably reduces the differences between these times for large- and inertial-range scales. Indeed, below the dissipative range, it appears that Φ has self-similar evolution for times such that the \hat{k}^{-3} law applies. That this requires sufficiently large \hat{t} is illustrated by the results for $\hat{t} = 5$. Figures 4(b) and 4(c) suggest that $\Phi_{\perp}(\hat{k}_{\perp})$ and $\Phi_{\parallel}(\hat{k}_{\parallel})$ are also self-similar in the large- and inertial-scale ranges for large enough \hat{t} .

Self-similarity of Φ , Φ_{\perp} and Φ_{\parallel} suggests that the three-dimensional energy distribution, $\hat{e}(\hat{\mathbf{k}})$, is itself self-similar, i.e. (3.7) applies outside the dissipative range and for sufficiently large \hat{t} . As a test of this hypothesis, figure 5 shows contour plots of $\ell^{-3}\hat{e}$ in the $\hat{k}_{\perp}\ell-\hat{k}_{\parallel}\ell$ plane for $\hat{t} = 25$ and $\hat{t} = 50$. The wiggles in the curves are due to the use of a single realisation and illustrate the difficulties of using DNS to obtain definitive results for $\hat{e}(\hat{\mathbf{k}})$. Nonetheless, figure 5 appears to support the hypothesis of self-similarity of $\hat{e}(\hat{\mathbf{k}})$, away from the vertical axis, $\hat{k}_{\perp} = 0$. That such self-similarity cannot apply on the axis is apparent from our analytical demonstration that $\hat{e}(\hat{\mathbf{k}})$ is there determined by linear theory, hence dissipation alone. Since the large-scale dissipation is very small, the axial $\hat{e}(\hat{\mathbf{k}})$ is nearly time-independent. As a result, there is a near-axial region, perhaps of extent which tends to zero as $\hat{t} \rightarrow \infty$, in which self-similarity does not apply.

To study the effects of changing the initial conditions, we performed calculations using the initial conditions (3.8) with $\alpha = 1/2$ and $\alpha = 2$. Overall, the results agree with the case $\alpha = 1$ considered above and they suggest that the self-similar result of time evolution is independent of the initial conditions. If true, the function F in (3.9) is universal.

The contours of constant $\ell^{-3}\hat{e}$ in figures 5 and 7 are non-circular, even away from the axis, which suggests that $\hat{e}(\hat{\mathbf{k}})$ is anisotropic. The results for the inertial range indicate a preference for energy transfer in the vertical direction. Despite anisotropy, we found approximate Charney equipartition of kinetic and potential energies at sufficiently large times, as indicated by figure 6. How such equipartition arises without the underlying isotropy is unclear.

Concerning the inertial range, although the self-similar energy distribution is anisotropic, we found that it could be made approximately Charney isotropic by using the variable $\beta_0^{-1}\hat{k}_3$, rather than \hat{k}_3 , where $\beta_0 = 1.4$. This leads to (3.12) for the inertial-range energy distribution in \mathbf{k} -space at sufficiently large times and away from the vertical axis. This distribution is isotropic in the usual sense when $\beta = \beta_0$, but not for other values of β . Note that such isotropy in \mathbf{k} -space for $\beta = \beta_0$ does not imply agreement with the prediction of isotropy in $\hat{\mathbf{k}}$ -space by [II]. The distribution in $\hat{\mathbf{k}}$ -space is always anisotropic and given by (3.11), which is, of course, independent of β .

A further significant result concerns the time dependence of the measures, ℓ , ℓ_\perp and ℓ_\parallel , of the size of the large scales, whose temporal evolution is shown in figure 8. They seem to follow a $\hat{t}^{1/2}$ power law in the range of time for which we expect self-similarity.

To summarise, following a phase in which energy transfer from large to small scales creates an inertial range, then a dissipative one, we find that considerable further evolution is needed before the proposals of [II] are applicable. The results show near conservation of energy and growth in size of the large scales, both of which are indicative of the inverse energy cascade proposed by [II]. They also agree with the k^{-3} inertial-range spectrum and (approximately) with the equipartition of kinetic and potential energies suggested by [II].

However, our results also suggest that the assumption of isotropy by [II] is incorrect and further indicate self-similarity of the time evolution of the spectral energy distribution away from the vertical axis and at large enough times. Self-similarity, the k^{-3} spectrum and approximate equipartition appear at about the same time, which suggests they are related.

Following our work, one might ask why equipartition appears to be (approximately) respected by the self-similar flow, although Charney isotropy, from which equipartition was deduced in [II], is not. It would also be interesting to better understand the lack of self-similarity near the vertical axis. Finally, a theoretical understanding of the apparent long-time $\hat{t}^{1/2}$ dependence of the size of the large scales is lacking, as is an explanation of the observed value of the scaling factor, $\beta_0 = 1.4$, which appears to make the inertial-range, self-similar energy distribution in \mathbf{k} -space isotropic for $\beta = \beta_0$.

Declaration of interests. The authors report no conflict of interest.

Appendix A: The three-dimensional QG problem and derivation of (2.23) and (2.24)

Define the potential vorticity by

$$q = \frac{\partial u_2^{NP}}{\partial x_1} - \frac{\partial u_1^{NP}}{\partial x_2} - \beta \frac{\partial \eta^{NP}}{\partial x_3}, \quad (\text{A1})$$

whose Fourier transform gives

$$\tilde{q} = i \left(k_1 \widetilde{u_2^{NP}} - k_2 \widetilde{u_1^{NP}} - \beta k_3 \widetilde{\eta^{NP}} \right). \quad (\text{A2})$$

The inverse Fourier transforms of (2.21) and (2.22) give $\widetilde{u_i^{NP}} = a_0 v_i^{(0)}$, $\widetilde{\eta^{NP}} = a_0 \eta^{(0)}$. Using this result, (2.17), (2.18) and (A2),

$$\tilde{q} = (k_1^2 + k_2^2 + \beta^2 k_3^2)^{1/2} a_0. \quad (\text{A3})$$

The Fourier inverse of (A3) gives (2.24).

Define ψ via its Fourier transform

$$\tilde{\psi} = -(k_1^2 + k_2^2 + \beta^2 k_3^2)^{-1/2} a_0. \quad (\text{A4})$$

Given $\widetilde{u_i^{NP}} = a_0 v_i^{(0)}$, $\widetilde{\eta^{NP}} = a_0 \eta^{(0)}$, (2.17), (2.18) and (A4) yield

$$\widetilde{u_1^{NP}} = -i k_2 \tilde{\psi}, \quad \widetilde{u_2^{NP}} = i k_1 \tilde{\psi}, \quad \widetilde{u_3^{NP}} = 0, \quad \widetilde{\eta^{NP}} = -i \beta k_3 \tilde{\psi}, \quad (\text{A5})$$

while (A3) and (A4) give

$$\tilde{q} = -(k_1^2 + k_2^2 + \beta^2 k_3^2) \tilde{\psi}. \quad (\text{A6})$$

The inverse Fourier transforms of (A5) and (A6) imply

$$u_1^{NP} = -\frac{\partial \psi}{\partial x_2}, \quad u_2^{NP} = \frac{\partial \psi}{\partial x_1}, \quad u_3^{NP} = 0, \quad \eta^{NP} = -\beta \frac{\partial \psi}{\partial x_3}, \quad (\text{A7})$$

and

$$q = \frac{\partial^2 \psi}{\partial x_1^2} + \frac{\partial^2 \psi}{\partial x_2^2} + \beta^2 \frac{\partial^2 \psi}{\partial x_3^2}. \quad (\text{A8})$$

Equations (2.19), (2.20), (A3) and (A4) imply

$$\begin{aligned} \frac{\partial \tilde{q}}{\partial t} - k^2 (D_u (k_1^2 + k_2^2) + D_\eta \beta^2 k_3^2) \tilde{\psi} \\ = -i (k_1^2 + k_2^2 + \beta^2 k_3^2)^{1/2} k_j (v_i^{(0)*} \widetilde{u_i^{NP} u_j^{NP}} + \eta^{(0)*} \widetilde{\eta^{NP} u_j^{NP}}). \end{aligned} \quad (\text{A9})$$

Employing (2.17) and (2.18),

$$\begin{aligned} (k_1^2 + k_2^2 + \beta^2 k_3^2)^{1/2} (v_i^{(0)*} \widetilde{u_i^{NP} u_j^{NP}} + \eta^{(0)*} \widetilde{\eta^{NP} u_j^{NP}}) \\ = -i (k_2 \widetilde{u_1^{NP} u_j^{NP}} - k_1 \widetilde{u_2^{NP} u_j^{NP}} + \beta k_3 \widetilde{\eta^{NP} u_j^{NP}}), \end{aligned} \quad (\text{A10})$$

which is used to express the right-hand side of (A9). Taking the inverse Fourier transform

$$\begin{aligned} \frac{\partial q}{\partial t} - \nabla^2 \left(D_u \left(\frac{\partial^2 \psi}{\partial x_1^2} + \frac{\partial^2 \psi}{\partial x_2^2} \right) + D_\eta \beta^2 \frac{\partial^2 \psi}{\partial x_3^2} \right) \\ = \frac{\partial}{\partial x_j} \left(\frac{\partial}{\partial x_2} (u_1^{NP} u_j^{NP}) - \frac{\partial}{\partial x_1} (u_2^{NP} u_j^{NP}) + \beta \frac{\partial}{\partial x_3} (\eta^{NP} u_j^{NP}) \right). \end{aligned} \quad (\text{A11})$$

Given $\widetilde{u_i^{NP}} = a_0 v_i^{(0)}$, (2.17) implies $k_j \widetilde{u_j^{NP}} = 0$, hence $\partial u_j^{NP} / \partial x_j = 0$. Using this result, the right-hand side of (A11) can be rewritten as

$$\begin{aligned} & \frac{\partial}{\partial x_2} \left(u_j^{NP} \frac{\partial u_1^{NP}}{\partial x_j} \right) - \frac{\partial}{\partial x_1} \left(u_j^{NP} \frac{\partial u_2^{NP}}{\partial x_j} \right) + \beta \frac{\partial}{\partial x_3} \left(u_j^{NP} \frac{\partial \eta^{NP}}{\partial x_j} \right) \\ &= \frac{\partial u_j^{NP}}{\partial x_2} \frac{\partial u_1^{NP}}{\partial x_j} - \frac{\partial u_j^{NP}}{\partial x_1} \frac{\partial u_2^{NP}}{\partial x_j} + \beta \frac{\partial u_j^{NP}}{\partial x_3} \frac{\partial \eta^{NP}}{\partial x_j} \\ &+ u_j^{NP} \frac{\partial}{\partial x_j} \left(\frac{\partial u_1^{NP}}{\partial x_2} - \frac{\partial u_2^{NP}}{\partial x_1} + \beta \frac{\partial \eta^{NP}}{\partial x_3} \right). \end{aligned} \quad (\text{A12})$$

Since $u_3^{NP} = 0$, the first term on the right-hand side of (A12) gives

$$\frac{\partial u_j^{NP}}{\partial x_2} \frac{\partial u_1^{NP}}{\partial x_j} = \frac{\partial u_1^{NP}}{\partial x_2} \frac{\partial u_1^{NP}}{\partial x_1} + \frac{\partial u_2^{NP}}{\partial x_2} \frac{\partial u_1^{NP}}{\partial x_2} = \frac{\partial u_1^{NP}}{\partial x_2} \left(\frac{\partial u_1^{NP}}{\partial x_1} + \frac{\partial u_2^{NP}}{\partial x_2} \right) = 0, \quad (\text{A13})$$

where we have again used $\partial u_j^{NP} / \partial x_j = 0$. Similar reasoning implies that the second term on the right-hand side of (A12) is also zero, while, using (A7), the third term can be rewritten as

$$\beta \frac{\partial u_j^{NP}}{\partial x_3} \frac{\partial \eta^{NP}}{\partial x_j} = \beta^2 \left(\frac{\partial^2 \psi}{\partial x_2 \partial x_3} \frac{\partial^2 \psi}{\partial x_1 \partial x_3} - \frac{\partial^2 \psi}{\partial x_1 \partial x_3} \frac{\partial^2 \psi}{\partial x_2 \partial x_3} \right) = 0. \quad (\text{A14})$$

Thus, only the final term of (A12) is non-zero. Using (A1) to express that term, (A11) gives

$$\frac{\partial q}{\partial t} + u_j^{NP} \frac{\partial q}{\partial x_j} = \nabla^2 \left(D_u \left(\frac{\partial^2 \psi}{\partial x_1^2} + \frac{\partial^2 \psi}{\partial x_2^2} \right) + D_\eta \beta^2 \frac{\partial^2 \psi}{\partial x_3^2} \right). \quad (\text{A15})$$

Equations (A7), (A8) and (A15) form the three-dimensional QG equations with constant density and Brunt–Vaisala frequency. To see this, we refer to [II], in particular equation (8) of that article. Note that the notation β has different meanings in [II] and the present work. The work in [II] uses β to refer to a β -plane effect which is not present in our problem, hence his β should be taken as zero. Note also that equation (8) of [II] does not include visco-diffusion, represented by the right-hand side of equation (A15).

Since $\partial u_j^{NP} / \partial x_j = 0$, (A15) implies

$$\frac{\partial q}{\partial t} + \frac{\partial}{\partial x_j} (u_j^{NP} q) = \nabla^2 \left(D_u \left(\frac{\partial^2 \psi}{\partial x_1^2} + \frac{\partial^2 \psi}{\partial x_2^2} \right) + D_\eta \beta^2 \frac{\partial^2 \psi}{\partial x_3^2} \right). \quad (\text{A16})$$

Taking the Fourier transform of (A16) and using (2.19), (A3) and (A4) gives (2.23).

Appendix B: Numerical method

The flow is approximated as periodic with respect to x_1 , x_2 and x_3 . Thus, (2.36) and (2.37) are replaced by the Fourier series

$$\hat{u}_i = \sum_{\hat{\mathbf{k}}} b(\hat{\mathbf{k}}) v_i^{(0)}(\hat{\mathbf{k}}) \exp(i\hat{\mathbf{k}} \cdot \hat{\mathbf{x}}), \quad (\text{B1})$$

$$\hat{q} = \sum_{\hat{\mathbf{k}}} \hat{k} b(\hat{\mathbf{k}}) \exp(i\hat{\mathbf{k}} \cdot \hat{\mathbf{x}}), \quad (\text{B2})$$

in which the sums are over $\hat{\mathbf{k}}$ having components $\hat{k}_1 = 2\pi l_1/L_1$, $\hat{k}_2 = 2\pi l_2/L_2$, $\hat{k}_3 = 2\pi l_3/L_3$, where the l_i take integer values and L_i are the spatial periods. As usual in DNS, the spatial periods, L_i , need to be sufficiently large that periodicity is unimportant. Another way of putting this is that the spacing, $2\pi/L_i$, in spectral space should be sufficiently small. The numerical equivalent of (2.35) is

$$\frac{db}{d\hat{t}} + \hat{D}b = -i\hat{k}^{-1} \hat{k}_j \widetilde{\hat{u}_j \hat{q}}, \quad (\text{B3})$$

with suitable interpretation of $\widetilde{\hat{u}_j \hat{q}}$ in terms of discrete Fourier transforms.

The quantity $v_i^{(0)}(\hat{\mathbf{k}})$ in (B1) is given by (2.32). There is, however, a problem with both (2.32) and (B3) when $\hat{\mathbf{k}} = 0$, namely a zero-by-zero division, which is resolved as follows. The $\hat{\mathbf{k}} \rightarrow 0$ limit of (2.20) implies

$$\frac{\partial a_0}{\partial t} + D_{00}a_0 = 0, \quad (\text{B4})$$

for $\hat{\mathbf{k}} = 0$. We specialise to initial conditions such that $a_0(\hat{\mathbf{k}} = 0) = 0$, hence (B4) indicates that this is true at all later times. The numerical equivalent of this result is $b(\hat{\mathbf{k}} = 0) = 0$, which we assume to hold. Thus, the $\hat{\mathbf{k}} = 0$ term in (B1) is zero and (B3) need only be applied for $\hat{\mathbf{k}} \neq 0$, hence avoiding zero-by-zero division.

In addition to supposing periodicity, the sums in (B1) and (B2) are truncated to $|l_i| \leq K_i$, where K_i are positive integers, which must be sufficiently large that the smallest dynamically significant length scales of the flow are resolved. Evaluating (B1) and (B2) at the discrete points $\hat{x}_1 = p_1 L_1/N_1$, $\hat{x}_2 = p_2 L_2/N_2$, $\hat{x}_3 = p_3 L_3/N_3$, where $N_i > 2K_i$ and $0 \leq p_i < N_i$ are integers, the result can be expressed as

$$\hat{u}_i = \sum_{s_1=0}^{N_1-1} \sum_{s_2=0}^{N_2-1} \sum_{s_3=0}^{N_3-1} \xi_i(s_1, s_2, s_3) \exp\left(2\pi i \left(\frac{s_1 p_1}{N_1} + \frac{s_2 p_2}{N_2} + \frac{s_3 p_3}{N_3}\right)\right), \quad (\text{B5})$$

$$\hat{q} = \sum_{s_1=0}^{N_1-1} \sum_{s_2=0}^{N_2-1} \sum_{s_3=0}^{N_3-1} \xi(s_1, s_2, s_3) \exp\left(2\pi i \left(\frac{s_1 p_1}{N_1} + \frac{s_2 p_2}{N_2} + \frac{s_3 p_3}{N_3}\right)\right), \quad (\text{B6})$$

in which $\xi_i = \xi = 0$ unless $s_i \leq K_i$ or $s_i \geq N_i - K_i$. Otherwise,

$$\xi_i(s_1, s_2, s_3) = b(\hat{\mathbf{k}}) v_i^{(0)}(\hat{\mathbf{k}}), \quad (\text{B7})$$

$$\xi(q_1, q_2, q_3) = \hat{k} b(\hat{\mathbf{k}}), \quad (\text{B8})$$

where $\hat{\mathbf{k}} = 2\pi(l_1/L_1, l_2/L_2, l_3/L_3)$, $l_i = s_i$ when $s_i \leq K_i$ and $l_i = s_i - N_i$ for $s_i \geq N_i - K_i$. Equations (B5) and (B6) are discrete Fourier transforms which are evaluated using the fast Fourier transform (FFT) algorithm.

Having determined \hat{u}_i and \hat{q} in physical space, the product $\hat{u}_j \hat{q}$ can be calculated. Performing the discrete Fourier transform inverse to (B5) and (B6)

$$\chi_j(s_1, s_2, s_3) = \frac{1}{N_1 N_2 N_3} \sum_{p_1=0}^{N_1-1} \sum_{p_2=0}^{N_2-1} \sum_{p_3=0}^{N_3-1} \hat{u}_j \hat{q}(p_1, p_2, p_3) \times \exp\left(-2\pi i \left(\frac{s_1 p_1}{N_1} + \frac{s_2 p_2}{N_2} + \frac{s_3 p_3}{N_3}\right)\right), \quad (\text{B9})$$

the nonlinear term in (B3) follows from

$$\widetilde{\hat{u}_j \hat{q}}(l_1, l_2, l_3) = \chi_j(s_1, s_2, s_3), \quad (\text{B10})$$

where $s_i = l_i$ for $0 \leq l_i \leq K_i$ and $s_i = N_i + l_i$ for $-K_i \leq l_i < 0$. As for (B5) and (B6), FFT is used to evaluate (B9).

Writing the evolution equation (B3) as

$$\frac{db}{d\hat{t}} + \hat{D}b = \gamma, \quad (\text{B11})$$

a time-stepping scheme is introduced. Time is discretised to the values $\hat{t}_n = n\Delta$, where Δ is the time step, and (B11) gives

$$b(\hat{t}_{n+1}) = b(\hat{t}_n) \exp(-\hat{D}\Delta) + \int_{\hat{t}_n}^{\hat{t}_{n+1}} \gamma(\hat{t}') \exp(\hat{D}(\hat{t}' - \hat{t}_{n+1})) d\hat{t}'. \quad (\text{B12})$$

Given $b(\hat{t}_n)$, $\gamma(\hat{t}_n)$ is determined using FFT as described above. As a first approximation, $\gamma(\hat{t}')$ is taken as constant and equal to $\gamma(\hat{t}_n)$, hence

$$b^\dagger = b(\hat{t}_n) \exp(-\hat{D}\Delta) + \gamma(\hat{t}_n) \frac{1 - \exp(-\hat{D}\Delta)}{\hat{D}}, \quad (\text{B13})$$

as an approximate value of $b(\hat{t}_{n+1})$. To increase the precision to second order, let γ^\dagger be the value obtained using $(b(\hat{t}_n) + b^\dagger)/2$, which approximates the value of $b(\hat{t})$ at time $\hat{t}_n + \Delta/2$. Thus,

$$b(\hat{t}_{n+1}) = b(\hat{t}_n) \exp(-\hat{D}\Delta) + \gamma^\dagger \frac{1 - \exp(-\hat{D}\Delta)}{\hat{D}}, \quad (\text{B14})$$

completes the time step. Note that, as \hat{k} increases, so does $\hat{D}(\hat{k})$, and, when $\hat{D}(\hat{k})\Delta$ becomes of $O(1)$, dissipative effects are significant within a time step. The above scheme maintains precision in this case, provided $b(\hat{t})$, and hence $\gamma(\hat{t})$, does not change too much over a single step. The scheme is an example of a general class, known as integrating factor methods (see e.g. Minchev & Wright (2005)).

The numerical equivalent of (2.38) is

$$\hat{\eta} = \sum_{\hat{\mathbf{k}}} b(\hat{\mathbf{k}}) \eta^{(0)}(\hat{\mathbf{k}}) \exp(i\hat{\mathbf{k}} \cdot \hat{\mathbf{x}}). \quad (\text{B15})$$

Using (B1) and (B15), as well as their complex conjugates,

$$\frac{1}{2} (\overline{\hat{u}_i \hat{u}_i} + \hat{\eta}^2) = \frac{1}{2} \sum_{\hat{\mathbf{k}}, \hat{\mathbf{k}}'} \overline{b^*(\hat{\mathbf{k}}) b(\hat{\mathbf{k}}')} (v_i^{(0)*}(\hat{\mathbf{k}}) v_i^{(0)}(\hat{\mathbf{k}}') + \eta^{(0)*}(\hat{\mathbf{k}}) \eta^{(0)}(\hat{\mathbf{k}}')) \times \exp(i(\hat{\mathbf{k}}' - \hat{\mathbf{k}}) \cdot \hat{\mathbf{x}}), \quad (\text{B16})$$

gives the average energy per unit volume. Statistical homogeneity means that (B16) should be independent of $\hat{\mathbf{x}}$, hence $b^*(\hat{\mathbf{k}})b(\hat{\mathbf{k}}') = 0$ for $\hat{\mathbf{k}}' \neq \hat{\mathbf{k}}$. Thus,

$$\frac{1}{2}(\overline{\hat{u}_i \hat{u}_i} + \overline{\hat{\eta}^2}) = \frac{1}{2} \sum_{\hat{\mathbf{k}}} \overline{|b|^2(\hat{\mathbf{k}})} \left(v_i^{(0)*}(\hat{\mathbf{k}}) v_i^{(0)}(\hat{\mathbf{k}}) + |\eta^{(0)}|^2(\hat{\mathbf{k}}) \right). \quad (\text{B17})$$

Using (2.32)

$$\frac{1}{2}(\overline{\hat{u}_i \hat{u}_i} + \overline{\hat{\eta}^2}) = \frac{1}{2} \sum_{\hat{\mathbf{k}}} \overline{|b|^2(\hat{\mathbf{k}})}, \quad (\text{B18})$$

which shows that the energy contribution of wave vector $\hat{\mathbf{k}}$ is $\overline{|b|^2(\hat{\mathbf{k}})}/2$.

Recalling that the spatial periods, L_i , should be large (in principle, tending to infinity) to avoid significant effects of periodicity, the density, $L_1 L_2 L_3 / 8\pi^3$, of discrete wave vectors in spectral space is also large. Thus, we interpret the sum in (B18) as a numerical approximation of the integral in (2.40), leading to

$$\hat{e}(\hat{\mathbf{k}}) = \frac{L_1 L_2 L_3}{16\pi^3} \overline{|b|^2(\hat{\mathbf{k}})}, \quad (\text{B19})$$

as the energy density in $\hat{\mathbf{k}}$ -space.

Equation (B19) is used in the initialisation of the DNS. The initial conditions for $b(\hat{\mathbf{k}})$ are subject to some constraints. In particular, they are of zero mean and, in order that the resulting flow be real, $b(-\hat{\mathbf{k}}) = b^*(\hat{\mathbf{k}})$. Supposing that the initial $\hat{e}(\hat{\mathbf{k}})$ is given and is non-negative and such that $\hat{e}(-\hat{\mathbf{k}}) = \hat{e}(\hat{\mathbf{k}})$, the calculation is initialised according to (B19) using

$$b(\hat{\mathbf{k}}) = \left(\frac{16\pi^3}{L_1 L_2 L_3} \hat{e}(\hat{\mathbf{k}}) \right)^{1/2} \exp(i\psi(\hat{\mathbf{k}})), \quad (\text{B20})$$

where the phases $\psi(\hat{\mathbf{k}})$ are random variables, uniformly distributed between $-\pi$ and π and independent apart from the reality constraint $\psi(-\hat{\mathbf{k}}) = -\psi(\hat{\mathbf{k}})$.

Once the $b(\hat{\mathbf{k}})$ have been calculated, we want to extract results. However, as noted in the main text, there is a problem. The accurate calculation of ensemble averages, such as $\overline{|b|^2(\hat{\mathbf{k}})}$, would require an impracticably large number of DNS runs. Thus, we consider a single run and suppose the results are representative of the average. The total energy is determined using

$$\hat{E}_{NP} = \frac{1}{2} \sum_{\hat{\mathbf{k}}} |b|^2(\hat{\mathbf{k}}), \quad (\text{B21})$$

rather than (B18), while (2.42), (2.43) and (3.5) lead to

$$\hat{E}_K = \frac{1}{2} \sum_{\hat{\mathbf{k}}} \frac{\hat{k}_1^2 + \hat{k}_2^2}{\hat{k}^2} |b|^2(\hat{\mathbf{k}}), \quad \hat{E}_P = \frac{1}{2} \sum_{\hat{\mathbf{k}}} \frac{\hat{k}_3^2}{\hat{k}^2} |b|^2(\hat{\mathbf{k}}), \quad (\text{B22})$$

$$\begin{pmatrix} \ell^{-1} \\ \ell_{\perp}^{-1} \\ \ell_{\parallel}^{-1} \end{pmatrix} = \frac{1}{2} \hat{E}_{NP}^{-1} \sum_{\hat{\mathbf{k}}} |b|^2(\hat{\mathbf{k}}) \begin{pmatrix} \hat{k} \\ \hat{k}_{\perp} \\ |\hat{k}_3| \end{pmatrix}. \quad (\text{B23})$$

Note that, to avoid zero-by-zero division and recalling that $b(\hat{\mathbf{k}} = 0) = 0$, the $\hat{\mathbf{k}} = 0$ term in the sums of (B22) is dropped.

From here on, we make the simplifying assumption that $L_1 = L_2 = L_3 = L$ and $K_1 = K_2 = K_3 = K$. Here, $\Phi(\hat{\mathbf{k}})$ is determined by considering the energy contained in the spherical shell $S(m)$ defined by $\hat{k}_m \leq \hat{k} < \hat{k}_{m+1}$ in $\hat{\mathbf{k}}$ -space, where $0 \leq m \leq K$ takes integer values and

$$\hat{k}_m = \frac{\pi}{L}(2m - 1). \quad (\text{B24})$$

Thus, dividing the energy in $S(m)$ by its thickness, $2\pi/L$,

$$\Phi(\hat{\mathbf{k}}) = \frac{L}{4\pi} \sum_{\hat{\mathbf{k}} \in S(m)} |b(\hat{\mathbf{k}})|^2 \quad (\text{B25})$$

gives Φ at the shell mid-point

$$\hat{k} = \frac{2\pi}{L}m \quad 0 \leq m \leq K. \quad (\text{B26})$$

Φ_{\perp} and Φ_{\parallel} are determined in the much the same way. Let $S_{\perp}(m)$ denote the region $\hat{k}_m \leq \hat{k}_{\perp} < \hat{k}_{m+1}$, then

$$\Phi_{\perp}(\hat{k}_{\perp}) = \frac{L}{4\pi} \sum_{\hat{\mathbf{k}} \in S_{\perp}(m)} |b(\hat{\mathbf{k}})|^2, \quad (\text{B27})$$

provides Φ_{\perp} for

$$\hat{k}_{\perp} = \frac{2\pi}{L}m \quad 0 \leq m \leq K. \quad (\text{B28})$$

Similarly, let $S_{\parallel}(m)$ denote the region $\hat{k}_m \leq \hat{k}_{\parallel} < \hat{k}_{m+1}$, then

$$\Phi_{\parallel}(\hat{k}_{\parallel}) = \frac{L}{4\pi} \sum_{\hat{\mathbf{k}} \in S_{\parallel}(m)} |b(\hat{\mathbf{k}})|^2, \quad (\text{B29})$$

gives Φ_{\parallel} for

$$\hat{k}_{\parallel} = \frac{2\pi}{L}m \quad 0 \leq m \leq K. \quad (\text{B30})$$

The energy distribution, $\hat{e}(\hat{\mathbf{k}})$, is approximated as follows. Statistical axisymmetry of the flow prior to numerical discretisation is supposed, so $\hat{e}(\hat{\mathbf{k}}) = \hat{e}(\hat{k}_{\perp}, k_3)$. Define axisymmetric regions $D(m_{\perp}, m_{\parallel})$ in spectral space by $k_{m_{\perp}} \leq k_{\perp} < k_{m_{\perp}+1}$ and $k_{m_{\parallel}} \leq k_3 < k_{m_{\parallel}+1}$, where $0 \leq m_{\perp} \leq K$ and $0 \leq m_{\parallel} \leq K$. Let

$$B_{m_{\perp}m_{\parallel}} = \frac{L^3}{16\pi^3 N_{m_{\perp}m_{\parallel}}} \sum_{\hat{\mathbf{k}} \in D(m_{\perp}, m_{\parallel})} |b(\hat{\mathbf{k}})|^2, \quad (\text{B31})$$

where the sum is over discrete wave vectors inside $D(m_{\perp}, m_{\parallel})$ and $N_{m_{\perp}m_{\parallel}}$ is the number of such wave vectors (which is non-zero given the construction of $D(m_{\perp}, m_{\parallel})$). Taking

the average of (B31) and using (B19)

$$\overline{B_{m_\perp m_\parallel}} = \frac{1}{N_{m_\perp m_\parallel}} \sum_{\widehat{\mathbf{k}} \in D(m_\perp, m_\parallel)} \widehat{e}(\widehat{\mathbf{k}}). \quad (\text{B32})$$

If the region is small in the k_\perp – k_3 plane (large enough L), variations of $\widehat{e}(\widehat{\mathbf{k}})$ across $D(m_\perp, m_\parallel)$ can be neglected and the right-hand side of (B32) approximates $\widehat{e}(\widehat{\mathbf{k}})$ throughout the given region, hence

$$\widehat{e}(\widehat{\mathbf{k}}) = \overline{B_{m_\perp m_\parallel}}. \quad (\text{B33})$$

The problem is that, as noted earlier, it is not feasible to determine the ensemble average of $B_{m_\perp m_\parallel}$ using DNS. Thus, we take the right-hand side of (B31) as representative of $\widehat{e}(k_\perp, k_3)$ at

$$k_\perp = \frac{2\pi}{L} m_\perp \quad 0 \leq m_\perp \leq K, \quad (\text{B34})$$

$$k_3 = \frac{2\pi}{L} m_\parallel \quad 0 \leq m_\parallel \leq K. \quad (\text{B35})$$

The function $f(x)$ is determined as follows. Let $V(m)$ denote the region

$$\widehat{k}_m \leq (\widehat{k}_\perp^2 + \beta_0^{-2} \widehat{k}_3^2)^{1/2} < \widehat{k}_{m+1}, \quad (\text{B36})$$

then

$$\frac{L^3}{16\pi^3 \ell^3 N_m} \sum_{\widehat{\mathbf{k}} \in V(m)} |b(\widehat{\mathbf{k}})|^2 \quad (\text{B37})$$

gives the value of $f(x)$ at

$$x = \frac{2\pi \ell}{L} m \quad 0 \leq m \leq K, \quad (\text{B38})$$

where N_m is the number of discrete wave vectors in $V(m)$.

The numerical parameters used to obtain the results described in §3 are $N_i = 512$, $K_i = 255$, $L_i = 60$, $\Delta = 10^{-2}$ and $d = 10^{-6}$, where the hyperviscous damping factor is $\widehat{D} = d\widehat{k}^6$

REFERENCES

- BOFFETTA, G. & ECKE, R.E. 2012 Two-dimensional turbulence. *Annu. Rev. Fluid Mech.* **44**, 427–451.
 CHARNEY, J.G. 1948 On the scale of atmospheric motions. *Geofys. Publ. Oslo* **17** (2), 1–17.
 CHARNEY, J.G. 1971 Geostrophic turbulence. *J. Atmos. Sci.* **28**, 1087–1095.
 DRITSCHEL, D.G., DE LA TORRE JUAREZ, M. & AMBAUM, M.H.P. 1999 The three-dimensional vortical nature of atmospheric and oceanic turbulent flows. *Phys. Fluids* **11**, 1512–1520.
 HAUGEN, N.E.L. & BRANDENBURG, A. 2004 Inertial range scaling in numerical turbulence with hyperviscosity. *Phys. Rev. E* **70**, 026405.
 HUA, B.L. & HAIDVOGEL, D.B. 1986 Numerical simulations of the vertical structure of quasi-geostrophic turbulence. *J. Atmos. Sci.* **43**, 2923–2936.
 LOWE, A.J. & DAVIDSON, P.A. 2005 The evolution of freely-decaying, isotropic, two-dimensional turbulence. *Eur. J. Mech. B Fluids* **24**, 314–327.
 MCWILLIAMS, J.C. 1989 Statistical properties of decaying geostrophic turbulence. *J. Fluid Mech.* **198**, 199–230.
 MCWILLIAMS, J.C. 1990 The vortices of geostrophic turbulence. *J. Fluid Mech.* **219**, 387–404.

- MCWILLIAMS, J.C., WEISS, J.B. & YAVNEH, I. 1999 The vortices of homogeneous geostrophic turbulence. *J. Fluid Mech.* **401**, 1–26.
- MINCHEV, B.V. & WRIGHT, W.M. 2005 A review of exponential integrators for first order semi-linear problems. *Tech. Rep.*, NTNU.
- REINAUD, J.N., DRITSCHEL, D.G. & KOUDELLA, C.R. 2003 The shape of vortices in quasi-geostrophic turbulence. *J. Fluid Mech.* **474**, 175–192.
- RHINES, P.B. 1979 Geostrophic turbulence. *Annu. Rev. Fluid Mech.* **11**, 401–441.
- SAGAUT, P. & CAMBON, C. 2018 *Homogeneous Turbulence Dynamics*. 2nd edn. Springer.
- SCOTT, J.F. & CAMBON, C. 2024 Evolution of weak, homogeneous turbulence with rotation and stratification. *J. Fluid Mech.* **979**, A17.
- SCOTT, J.F. 2025 Evolution of weak, homogeneous turbulence subject to rotation and stratification: comparable wave and non-propagating components. *Phys. Rev. E* **111**, 035101.
- SMITH, L.M. & WALEFFE, F. 2002 Generation of slow large scales in forced rotating stratified turbulence. *J. Fluid Mech.* **451**, 145–168.
- VALLGREN, A. & LINDBORG, E. 2010 Charney isotropy and equipartition in quasi-geostrophic turbulence. *J. Fluid Mech.* **656**, 448–457.
- VON HARDENBERG, J., MCWILLIAMS, J.C., PROVENZALE, A., SHCHEPETKIN, A. & WEISS, J.B. 2000 Vortex merging in quasi-geostrophic flows. *J. Fluid Mech.* **412**, 331–353.